Inorganic Chemistry

ARTICLE

pubs.acs.org/IC

Monoanionic Molybdenum and Tungsten Tris(dithiolene) Complexes: A Multifrequency EPR Study

Stephen Sproules,*[,†] Priyabrata Banerjee,[†,§] Thomas Weyhermüller,[†] Yong Yan,[‡] James P. Donahue,*[,‡] and Karl Wieghardt*[,†]

[†]Max-Planck-Institut für Bioanorganische Chemie, Stiftstrasse 34-36, D-45470 Mülheim an der Ruhr, Germany

[‡]Department of Chemistry, Tulane University, 6400 Freret Street, New Orleans, Louisiana 70118-5698, United States

Supporting Information

ABSTRACT: Numerous Mo and W tris(dithiolene) complexes in varying redox states have been prepared and representative examples characterized crystallographically: $[M(S_2C_2R_2)_3]^z$ [M = Mo, R = Ph, $z = 0$ (**1**) or 1− (**2**); M = W, R = Ph, $z = 0$ (**4**) or 1− (**5**); R = CN, $z = 2-$, M = Mo (**3**) or W (**6**)]. Changes in dithiolene C−S and C−C bond lengths for **1** versus **2** and **4** versus **5** are indicative of ligand reduction. Trigonal twist angles (Θ) and dithiolene fold angles (α) increase and decrease, respectively, for **2** versus **1**, **5** versus **4**. Cyclic voltammetry reveals generally two reversible couples corresponding to 0/1− and 1−/2− reductions. The electronic structures of monoanionic molybdenum tris(dithiolene) complexes have been analyzed by multifrequency (S-, X-, Q-band) EPR spectroscopy. Spin-Hamiltonian parameters afforded by spectral simulation for each complex demonstrate the existence of two distinctive electronic structure types. The first is $[Mo^{IV}(^{A}L_3^{5-\bullet})]^{1-}$ (^{A}L = olefinic dithiolene, type A), which has the unpaired electron restricted to the tris(dithiolene) unit and is characterized by isotropic *g*-values and small molybdenum superhyperfine coupling. The second is formulated as $[Mo^{V}(^{B}L_3^{6-})]^{1-}$ (^{B}L = aromatic dithiolene, type B) with spectra distinguished by a prominent *g*-anisotropy and hyperfine coupling consistent with the $(d_{z^2})^1$ paramagnet. The electronic structure disparity is also manifested in their electronic absorption spectra. The compound $[W(bdt)_3]^{1-}$ exhibits spin-Hamiltonian parameters similar to those of $[Mo(bdt)_3]^{1-}$ and thus is formulated as $[W^{V}(^{B}L_3^{6-})]^{1-}$. The EPR spectra of $[W(^{A}L_3)]^{1-}$ display spin-Hamiltonian parameters that suggest their electronic structure is best represented by two resonance forms $\{[W^{IV}(^{A}L_3^{5-\bullet})]^{1-} \leftrightarrow [W^{V}(^{A}L_3^{6-})]^{1-}\}$. The contrast with the corresponding $[Mo^{IV}(^{A}L_3^{5-\bullet})]^{1-}$ complexes highlights tungsten's preference for higher oxidation states.

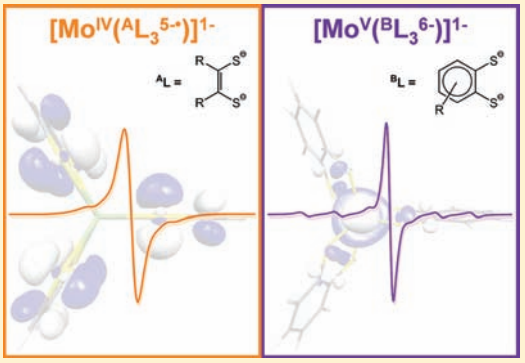

INTRODUCTION

When, in 1963, King combined the then novel organosulfur compound bis(trifluoromethyl)dithietene with molybdenum hexacarbonyl, the first tris(dithiolene) coordination complex was isolated.[1] The spectroscopic data led to its formulation as neutral $[Mo(tfd)_3]$, where $(tfd)^{2-}$ is bis(trifluoromethyl)-1,2-dithiolate. The first crystallographic characterization of a tris(dithiolene)molybdenum compound followed shortly after from the group of Schrauzer in Munich.[2] The MoS_6 polyhedron was found to be perfectly trigonal prismatic, and together with $[Re(pdt)_3]$, where $(pdt)^{2-}$ is 1,2-diphenyl-1,2-dithiolate, and $[V(pdt)_3]$ represented the only known nonoctahedral six-coordinate compounds.[3,4] Since these initial forays, tris(dithiolene) complexes of molybdenum have been the subject of the greatest number of synthetic and structural studies, with more than 25 reported crystal structures.[2,5−15] Together with this most unusual coordination geometry, interest in dithiolene chemistry was elicited by their facile redox chemistry and the formation of multimembered electron transfer series.[16] Molybdenum, and its group 6 congener tungsten, typically formed two- and three-membered series with a variety of dithiolene ligands.

Over the years their electronic structures were nearly always described as three closed-shell dianionic dithiolate ligands, $(L_3)^{6-}$, coordinated to a +IV, +V, and +VI central ion for the dianionic, monoanionic, and neutral complexes, respectively, such that the reversible redox processes are defined as metal-centered. It is interesting to note the ready acceptance of oxidized ligands in the analogous neutral vanadium compounds rather than entertainment of the notion of a +VI central ion; however, this option was only sparingly canvassed in the molybdenum and tungsten series. The relatively few studies that did postulate oxidized dithiolene ligands did so based on results from electron paramagnetic resonance (EPR) investigations of the paramagnetic $S = {}^1/_2$ monoanions.[17] With EPR, the location of the unpaired electron could be determined from both the *g*-value and the magnitude of the magnetic hyperfine interaction due to the presence of $^{95,97}Mo$ ($I = {}^5/_2$, 25.47% natural abundance) and (though to a considerably less degree) ^{183}W ($I = {}^1/_2$, 14.31% natural abundance) isotopes. This work led researchers to

Received: March 26, 2011
Published: June 23, 2011

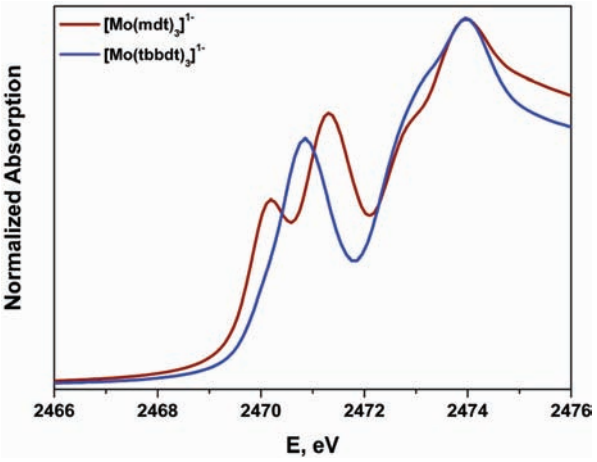

Figure 1. Overlay of the normalized S K-edge XAS spectra of $[Mo(mdt)_3]^{1-}$ (maroon) and $[Mo(tbbdt)_3]^{1-}$ (blue). Data are taken from refs 13 and 20.

Scheme 1. Dithiolene Ligand Types

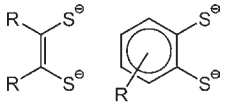

propose a $[Mo^{IV}(L_3^{5-\bullet})]^{1-}$ electronic structure,[17] where a diamagnetic Mo(IV) d^2 ion is coordinated by a singly oxidized tris(dithiolene) ligand set, $(L_3)^{5-\bullet}$. A single-crystal EPR experiment by Kwik and Stiefel confirmed that the neutral and dianionic members of the V(dithiolene)$_3$ series have the same d^1 electron configuration:[18] a V(IV) central ion in both species. Moreover, we have recently demonstrated the spectacular differences in the ^{185,187}Re ($I = {}^5/_2$, 100% natural abundance) hyperfine interactions in spectra of the neutral and dianionic members of the tris(dithiolene)rhenium series,[19] which unambiguously define the former as a ligand-centered paramagnet with a diamagnetic Re(V) d^2 central ion, while the latter possesses a Re(IV) d^3 ($S = {}^1/_2$) ion chelated by three closed-shell dianonic dithiolate ligands.

A recent, incisive X-ray absorption spectroscopic (XAS) and computational study by Solomon and co-workers revealed a variability to the electronic structures of the tris(dithiolene)-molybdenum complexes that was previously unrecognized.[20] By using sulfur K-edge XAS, it was shown when the spectra were overlaid (Figure 1) that $[Mo(mdt)_3]^{1-}$ (mdt = 1,2-dimethyl-1,2-dithiolene) and $[Mo(tbbdt)_3]^{1-}$ (tbbdt =3,5-di-*tert*-butylbenzene-1,2-dithiolate) have distinctly different electronic structures. Compounds with "olefinic" dithiolenes (type A, Scheme 1) are described as $[Mo^{IV}(^AL_3^{5-\bullet})]^{1-}$; in contrast the species with aromatic dithiolenes (type B, Scheme 1) are $[Mo^{V}(^BL_3^{6-})]^{1-}$. Thus, the former has its unpaired electron residing in a pure ligand-centered molecular orbital, whereas it is in a d orbital in the latter. It was further concluded by Solomon and co-workers that the diamagnetic neutral complexes have the same $[Mo^{IV}(^{A,B}L_3^{4-})]^0$ electronic structure, in stark contrast to our interpretation for $[Mo^{V}\{(tbbdt)_3^{5-\bullet}\}]^0$,[13] and the diamagnetic dianions, not unexpectedly, are formulated as $[Mo^{IV}(^{A,B}L_3^{6-})]^{2-}$.

Scheme 2. Ligands and Complexes

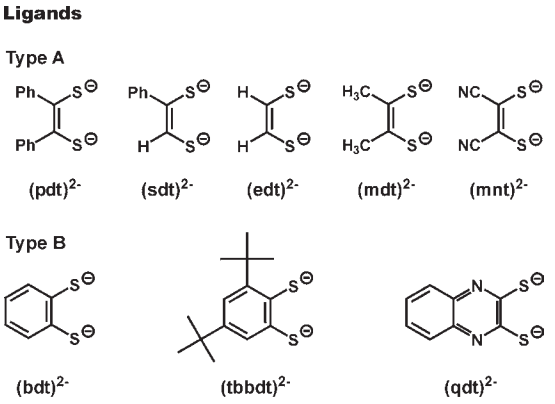

Complexes

$[Mo(pdt)_3]$	S = 0	**1**
$[PPh_4][Mo(pdt)_3]$	S = 1/2	**2**
$[PPh_4]_2[Mo(mnt)_3]$	S = 0	**3**
$[W(pdt)_3]$	S = 0	**4**
$[PPh_4][W(pdt)_3]$	S = 1/2	**5**
$[PPh_4]_2[W(mnt)_3]$	S = 0	**6**

Herein, we present a multifrequency (S-, X-, Q-band) EPR study of a broad array of monoanionic molybdenum and tungsten tris(dithiolene) complexes chelated by a selection of dithiolene ligands that encompasses both types (^{A}L and ^{B}L, Schemes 1 and 2). These results facilitate characterizing the two different electronic structures for the monoanions by their spin-Hamiltonian parameters and show how remarkably subtle the differences are when comparing to the aforementioned vanadium and rhenium analogues. Additionally, we examine the relationship between complex geometry determined by X-ray crystallography with these different electronic structures.

EXPERIMENTAL SECTION

Synthesis of Complexes. All air-sensitive materials were manipulated using standard Schlenk techniques or a glovebox. 4,5-Diphenyl-1,3-dithiol-2-one was prepared according to the method of Bhattacharya and Hortmann,[40] and $[PPh_4][BH_4]$ following the recipe of Makhaev et al.[21] The following complexes have been synthesized according to procedures described in the literature: $[NBu_4][Mo(bdt)_3]$;[9] $[PPh_4][Mo(qdt)_3]$;[6] $[NBu_4][Mo(tbbdt)_3]$;[13] $[Mo(edt)_3]^0$;[22] $[Mo(sdt)_3]^0$;[23] $[PPh_4]_2[Mo(mnt)_3]$ (**3**);[24] $[W(pdt)_3]^0$ (**4**);[25] $[PPh_4][W(bdt)_3]$;[26] $[NEt_4][W(mdt)_3]$;[12] $[PPh_4]_2[W(mnt)_3]$ (**6**).[24]

[Mo(pdt)$_3$] (1). A solution of $Cs(OH)\cdot H_2O$ (336 mg; 2.00 mmol) dissolved in MeOH (5 mL) was treated with 4,5-diphenyl-1,3-dithiol-2-one (270 mg; 0.998 mmol) and stirred for 10 min until it became pale yellow. The solution was cooled to −78 °C in an acetone/dry ice bath after which concentrated HCl (37%, 4.5 mL) was added followed by $Na_2MoO_4\cdot 2H_2O$ (70 mg, 0.29 mmol). The reaction mixture was slowly brought to room temperature with stirring over the course of an hour, and then air was bubbled through the solution to afford a green precipitate. The green solid was extracted into dichloromethane (10 mL) and washed with a saturated aqueous solution of $NaHCO_3$ (200 mL). The organic phase was separated, dried over $MgSO_4$, and filtered. The solvent was removed under vacuum to yield a dark green oily residue. This residue was dissolved in a minimum amount of CH_2Cl_2 and eluted on a silica gel column (Kieselgel 60, 230−400 mesh) with 1:1

dx.doi.org/10.1021/ic2006265 |*Inorg. Chem.* 2011, 50, 7106–7122

Table 1. Crystallographic Data for $1\cdot CH_2Cl_2$, $2\cdot CH_2Cl_2$, 3, $4\cdot CH_2Cl_2$, $5\cdot CH_2Cl_2$, 6, and $[NEt_4]_2[W(mdt)_3]$

	$1\cdot CH_2Cl_2$	$2\cdot CH_2Cl_2$	3	$4\cdot CH_2Cl_2$	$5\cdot CH_2Cl_2$	6	$[NEt_4]_2[W(mdt)_3]$
chem. formula	$C_{43}H_{32}Cl_2MoS_6$	$C_{67}H_{52}Cl_2MoPS_6$	$C_{60}H_{40}MoN_6P_2S_6$	$C_{43}H_{32}Cl_2S_6W$	$C_{67}H_{52}Cl_2PS_6W$	$C_{60}H_{40}N_6P_2S_6W$	$C_{28}H_{58}N_2S_6W$
fw	907.89	1247.26	1195.22	995.80	1335.17	1283.13	798.97
space group	$P\bar{1}$, No. 2	$P2_1/n$, No. 14	*Pbcn*, No. 60	$P\bar{1}$, No. 2	$P2_1/n$, No. 14	*Pbcn*, No. 60	$P2_1/c$, No. 14
a, Å	11.9102(6)	14.101(2)	19.846(3)	11.8989(4)	14.1851(6)	19.9080(3)	15.805(2)
b, Å	16.7887(9)	30.901(4)	15.115(3)	16.7354(6)	31.0048(12)	15.1931(3)	12.4941(14)
c, Å	22.286(2)	14.709(2)	18.293(3)	22.2817(8)	14.8110(6)	18.3256(3)	18.5463(2)
α, deg	108.470(4)	90	90	108.389(4)	90	90	90
β, deg	100.012(4)	116.543(2)	90	100.009(3)	116.597(3)	90	104.492(9)
γ, deg	97.854(4)	90	90	97.998(3)	90	90	90
V, Å	4073.7(5)	5733.7(13)	5487.4(16)	4056.1(2)	5824.6(4)	5542.84(16)	3545.8(7)
Z	4	4	4	4	4	4	4
T, K	100(2)	100(2)	100(2)	100(2)	100(2)	100(2)	100(2)
ρ calcd, g cm^{-3}	1.480	1.445	1.447	1.631	1.523	1.538	1.497
reflns collected/$2\Theta_{max}$	96 279/65.00	112 508/53.48	112 960/55.00	97 000/60.00	115 582/60.00	127 250/70.00	30 760/56.56
unique reflns/$I > 2\sigma(I)$	29 361/26 718	12 019/9949	6285/4799	23 613/19 692	16 917/15 858	12 210/9432	8400/7330
no. of params/restraints	968/16	719/21	339/0	959/10	722/16	339/0	348/0
λ, Å /*μ*(Kα), cm^{-1}	0.710 73/7.92	0.710 73/6.11	0.710 73/5.72	0.710 73/33.20	0.710 73/23.60	0.710 73/24.14	0.710 73/36.31
R1[a]/goodness of fit[b]	0.0329/1.029	0.0404/1.077	0.0325/1.197	0.0310/1.031	0.0439/1.062	0.0297/1.019	0.0265/1.033
wR2[c] ($I > 2\sigma(I)$)	0.0823	0.0971	0.0688	0.0730	0.1039	0.0644	0.0552
residual density, e Å^{-3}	+2.12/−1.24	+1.10/−0.70	+0.61/−0.58	+2.89/−1.25	+6.36/−1.35	+2.08/−2.18	+1.52/−0.90

[a] Observation criterion: $I > 2\sigma(I)$. $R1 = \Sigma||F_o| - |F_c||/\Sigma|F_o|$. [b] $GOF = [\Sigma[w(F_o^2 - F_c^2)^2]/(n-p)]^{1/2}$. [c] $wR2 = [\Sigma[w(F_o^2 - F_c^2)^2]/\Sigma[w(F_o^2)^2]]^{1/2}$ where $w = 1/\sigma^2(F_o^2) + (aP)^2 + bP$, $P = (F_o^2 + 2F_c^2)/3$.

CH_2Cl_2/hexane as eluent. The grass green fractions were collected, combined, and evaporated to dryness. The microcrystalline product was recrystallized from CH_2Cl_2/hexane. Yield: 109 mg (46%). The compound has been previously characterized.[22,25]

$[PPh_4][Mo(pdt)_3]$ (2). To a 50 mL Schlenk flask containing a THF (10 mL) solution of **1** (110 mg; 0.133 mmol) was added a solution of $[PPh_4][BH_4]$ (48 mg, 0.136 mmol) in MeCN (1 mL). The initially green reaction mixture rapidly turned dark brown. After stirring for 30 min, the mixture was filtered onto a solution of PPh_4Br (61 mg; 0.145 mmol) in MeOH (10 mL). The precipitate was collected by filtration, washed with methanol, and dried under vacuum. Yield: 101 mg (61%). Anal. Calcd for $C_{66}H_{50}PS_6Mo\cdot CH_2Cl_2$: C, 63.55; H, 4.04. Found: C, 63.32; H, 4.11.

$[PPh_4][W(pdt)_3]$ (5). A THF (10 mL) solution of **4** (100 mg; 0.109 mmol) was treated with *n*-BuLi (1.6 M in hexanes; 69 μL; 0.110 mmol) and stirred for 1 h. The solution was filtered into MeOH (10 mL) containing PPh_4Br (48 mg; 0.114 mmol) affording a chocolate brown microcrystalline solid. This was collected by filtration, washed with methanol, and dried under vacuum. Yield: 61 mg (42%). The compound has been previously characterized previously.[22,27]

X-ray Crystallographic Data Collection and Refinement of the Structures. Single crystals of $1\cdot CH_2Cl_2$, $2\cdot CH_2Cl_2$, **3**, $4\cdot CH_2Cl_2$, $5\cdot CH_2Cl_2$, **6**, and $[NEt_4]_2[W(mdt)_3]$ were coated with perfluoropolyether, picked up with nylon loops and were immediately mounted in the nitrogen cold stream of the diffractometers. Graphite monochromated Mo Kα radiation (λ = 0.710 73 Å) from a Mo-target rotating-anode X-ray source was used throughout. Final cell constants were obtained from least-squares fits of several thousand strong reflections. Intensity data were corrected for absorption using intensities of redundant reflections with the program SADABS.[28] The structures were readily solved by Patterson methods and subsequent difference Fourier techniques. The Siemens ShelXTL[29] software package was used for solution and artwork of the structures, and ShelXL97[30] was used for the refinement. All non-hydrogen atoms were anisotropically refined, and hydrogen atoms were placed at calculated positions and refined as riding atoms with isotropic displacement parameters. Crystallographic data of the compounds are listed in Table 1.

A phenyl ring of a pdt ligand (C45−C50) in the isostructural compounds $2\cdot CH_2Cl_2$ and $5\cdot CH_2Cl_2$ was found to be disordered by rotation. A split atom model was refined, giving an occupation ratio of about 0.66:0.34 and 0.58:0.42, respectively. SAME, EADP, and SADI restraints of ShelXL97 were used for the refinement. Disorder was also found for the dichloromethane molecules in all solvent containing compounds. Split atom models with constrained bond distances, angles, and displacement parameters were refined to account for the disorder.

EPR Measurements. X-band cw EPR measurements were performed on a Bruker E500 ELEXSYS spectrometer with a standard Bruker cavity (ER4102ST) and an Oxford Instruments helium flow cryostat (ESR 910). S-band and Q-band cw EPR measurements were recorded on a Bruker ESP 300E spectrometer with an S-band loop-gap resonator (Bruker design ER4118SPT with custom improvements) and a Bruker Q-band cavity (ER5106QT), both with Bruker flexline support and an Oxford Instruments helium cryostat (CF935). Microwave frequencies were measured with a Hewlett-Packard frequency counter (HP5352B), and the field control was calibrated with a Bruker NMR field probe (ER035M). The spectra were simulated with the Bruker XSOPHE suite.[31] Fluid solution spectra were simulated using a spin Hamiltonian of the form $\hat{H} = g\cdot\mu_B\cdot B\cdot S + \Sigma a\cdot S\cdot I$, where the weighted summation is over all naturally occurring Mo and W isotopes, respectively; the other parameters have their usual meanings. Satisfactory fits were achieved using a Lorentzian line shape with molecular tumbling accommodated by the isotropic liquids model given by $\sigma_\nu = a + bM_I + cM_I^2 + dM_I^3$. Randomly orientated EPR spectra were simulated following the spin Hamiltonian $\hat{H} = \mu_B\cdot\mathbf{g}\cdot\mathbf{B}\cdot\mathbf{S} + \Sigma\mathbf{S}\cdot\mathbf{A}\cdot\mathbf{I}$, where **g** and **A** are the 3 × 3 electron Zeeman and magnetic hyperfine interaction matrices, respectively. A Gaussian line shape and distribution of *g*- and *A*-values (strain) were employed to account for the line width variation. In complexes of trigonal symmetry (D_{3h}, D_3, C_{3h}), **g** and **A** are coaxial, so noncoincidence angles were excluded.

dx.doi.org/10.1021/ic2006265 |*Inorg. Chem.* 2011, 50, 7106–7122

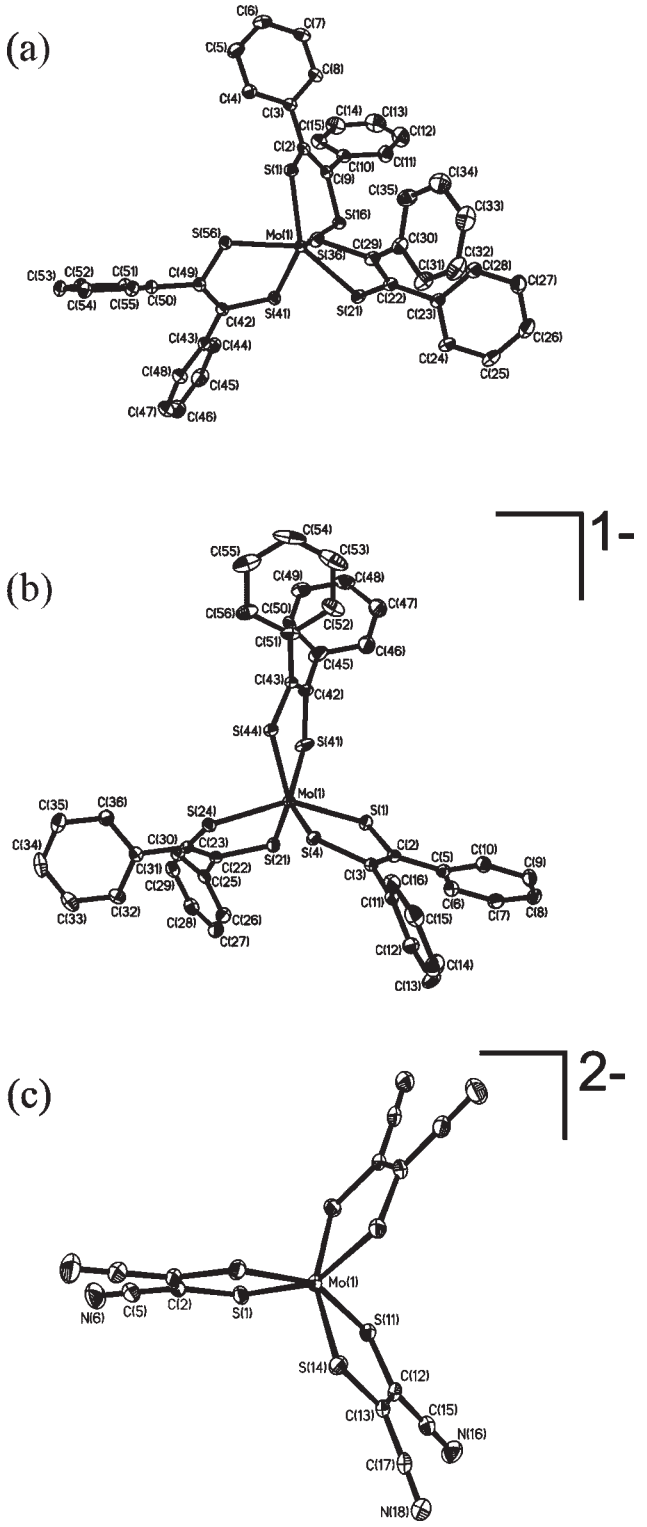

Figure 2. Structure of (a) the neutral molecule in crystals of **1**, (b) the monoanion in crystals of **2**, and (c) the dianion in crystals of **3**.

Other Physical Methods. Electronic absorption spectra of complexes from the spectroelectrochemical measurements were recorded on a HP 8452A diode array spectrophotometer (200−1100 nm). Cyclic voltammograms were recorded with an EG&G potentiostat/galvanostat. Elemental analyses were performed by H. Kolbe at the Mikroanalytischen Labor in Mülheim an der Ruhr, Germany.

Calculations. All calculations in this work were performed with the electronic structure program ORCA.[32] Geometry optimizations were carried out using the B3LYP functional.[33] A scalar relativistic correction was applied using the zeroth-order regular approximation (ZORA) method.[34b] In the context of ZORA, a one center approximation has been shown to introduce only minor errors to the final geometries.[34] An all-electron polarized triple-ζ-quality (def2-TZVP) basis set of Ahlrich's group was used for all atoms.[35] Auxiliary basis sets for all complexes used to expand the electron density in the calculations were chosen to match the orbital basis. The self-consistent field (SCF) calculations were tightly converged (1×10^{-8} E_h in energy, 1×10^{-7} E_h in the density change, and 1×10^{-7} in the maximum element of the DIIS[36] error vector). The geometry search for all complexes was carried out in redundant internal coordinates without imposing geometry constraints. Canonical orbitals and density plots were obtained using Molekel.[37]

RESULTS

1. Syntheses. Neutral $[Mo(pdt)_3]$ (**1**) was originally prepared by reacting $MoCl_5$ with the thiophosphate ester obtained in situ from the combination of benzoin and P_4S_{10} in refluxing dioxane.[22,38] However, our attempts to reproduce this preparation only led to the isolation of a dimeric molybdenum compound, $[\{Mo(pdt)(S_2P(OEt)_2)\}_2(\mu\text{-}S)\{(\mu)\text{-}\kappa^2\text{-}S_2\}]$,[39] whereas the analogous reaction with WCl_6 yielded the desired compound, $[W(pdt)_3]$ (**4**). Instead, we utilized a preparation adapted by Katakis and co-workers,[23] wherein 4,5-diphenyl-1,3-dithiol-2-one[40] is converted to the dicesium salt of 1,2-diphenyl-1,2-dithiolate, Cs_2pdt, by base hydrolysis with 2 equiv of cesium hydroxide. The salt generated in situ is cooled to −78 °C after which concentrated HCl is added followed by a suitable molybdenum precursor, in this case hydrated sodium molybdate. The dark green precipitate was collected and purified by column chromatography to afford **1** in reasonable yields.

Chemical reduction of **1** with tetraphenylphosphonium borohydride afforded $[PPh_4][Mo(pdt)_3]$ (**2**), while $[PPh_4][W(pdt)_3]$ (**5**) was generated by reduction of **4** with *n*-butyllithium and isolated as the tetraphenylphosphonium salt after addition of PPh_4Br. All other compounds were prepared according to the prescribed procedures.

2. Crystal Structure Determinations. The crystal structures of $\mathbf{1}\cdot CH_2Cl_2$ and $\mathbf{2}\cdot CH_2Cl_2$ have been determined by X-ray crystallography. The structures are shown in Figure 2, and selected bond distances and angles are summarized in Table 2.

The neutral species $[Mo(pdt)_3]$ (**1**) represents the eighth neutral molybdenum tris(dithiolene) complex to be structurally characterized (Table S1).[2,11,13,14] These complexes are distinguished by their trigonal prismatic array of six sulfur atoms about the molybdenum central ion and a pronounced dithiolene chelate fold to give, when viewed along the C_3 axis, a paddlewheel motif (Scheme 3). The structure of **1** is highly trigonal prismatic, with an average trigonal or "Bailar" twist angle (Θ_{av}) of 3.0° and large average fold angle (α_{av}) of 17.4°. The average C−S of 1.719 Å and C−C of 1.383 Å indicate a degree of dithiolene ligand oxidation, consistent with either an $(L_3)^{4-}$ or $(L_3)^{5-\bullet}$ ligand set. The average Mo−S distance is 2.3656 Å.

The structure of $\mathbf{2}\cdot CH_2Cl_2$ contains a monoanion, $[Mo(pdt)_3]^{1-}$, a well separated tetraphenylphosphonium cation (1:1), and one dichloromethane solvation molecule. The MoS_6 polyhedron is distorted trigonal prismatic ($\Theta_{av} = 18.0°$), and the fold angle reduced to 11.0°. The average intraligand C−S (1.739 Å) and C−C (1.355 Å) bond lengths are still shorter than a typical

dx.doi.org/10.1021/ic2006265 |*Inorg. Chem.* 2011, 50, 7106–7122

Table 2. Selected Bond Distances (Å) and Twist[a] (Θ, deg) and Fold Angles[a] (α, deg) in 1−6

Complex **1**·CH_2Cl_2					
Mo−S(1)	2.3650(4)	Mo−S(21)	2.3624(4)	Mo−S(41)	2.3730(4)
Mo−S(16)	2.3650(4)	Mo−S(36)	2.3686(4)	Mo−S(56)	2.3597(4)
S(1)−C(2)	1.717(1)	S(21)−C(22)	1.723(2)	S(41)−C(42)	1.721(1)
S(16)−C(9)	1.714(1)	S(36)−C(29)	1.722(2)	S(56)−C(49)	1.716(2)
C(2)−C(9)	1.385(2)	C(22)−C(29)	1.384(2)	C(42)−C(49)	1.380(2)
Θ_1	2.9°	Θ_2	3.2°	Θ_3	3.0°
α	17.8°	α′	23.9°	α″	10.4°
Complex **2**·CH_2Cl_2					
Mo−S(1)	2.3691(8)	Mo−S(21)	2.3452(8)	Mo−S(41)	2.3671(8)
Mo−S(4)	2.3745(8)	Mo−S(24)	2.3963(7)	Mo−S(44)	2.3881(7)
S(1)−C(2)	1.733(3)	S(21)−C(22)	1.736(3)	S(41)−C(42)	1.736(3)
S(4)−C(3)	1.741(3)	S(24)−C(23)	1.748(3)	S(44)−C(43)	1.740(3)
C(2)−C(3)	1.361(4)	C(22)−C(23)	1.356(4)	C(42)−C(43)	1.348(5)
Θ_1	19.1°	Θ_2	17.9°	Θ_3	17.0°
α	12.5°	α′	13.7°	α″	6.8°
Complex **3**					
Mo−S(1)	2.3742(7)	Mo−S(11)	2.3835(7)	Mo−S(14)	2.3889(7)
S(1)−C(2)	1.739(3)	S(11)−C(12)	1.733(3)	S(14)−C(13)	1.730(3)
C(2)−C(2)′	1.345(6)	C(12)−C(13)	1.360(4)		
Θ_1	25.5°	Θ_2	30.3°	Θ_3	30.3°
α	0.0°	α′	3.2°	α″	3.2°
Complex **4**·THF					
W−S(1)	2.3720(8)	W−S(21)	2.3716(9)	W−S(41)	2.3786(9)
W−S(4)	2.3752(9)	W−S(24)	2.3745(9)	W−S(44)	2.3691(9)
S(1)−C(2)	1.731(4)	S(21)−C(22)	1.734(4)	S(41)−C(42)	1.731(3)
S(4)−C(3)	1.733(3)	S(24)−C(23)	1.743(4)	S(44)−C(43)	1.738(4)
C(2)−C(3)	1.379(5)	C(22)−C(23)	1.384(5)	C(42)−C(43)	1.370(5)
Θ_1	3.0	Θ_2	3.5°	Θ_3	2.8°
α	20.2°	α′	26.1°	α″	12.7°
Complex **5**·CH_2Cl_2					
W−S(1)	2.3660(8)	W−S(21)	2.3785(9)	W−S(41)	2.3854(9)
W−S(4)	2.3799(10)	W−S(24)	2.3771(8)	W−S(44)	2.3916(8)
S(1)−C(2)	1.742(3)	S(21)−C(22)	1.745(3)	S(41)−C(42)	1.745(4)
S(4)−C(3)	1.770(4)	S(24)−C(23)	1.747(3)	S(44)−C(43)	1.743(4)
C(2)−C(3)	1.354(5)	C(22)−C(23)	1.362(5)	C(42)−C(43)	1.361(6)
Θ_1	23.3°	Θ_2	22.8°	Θ_3	22.2°
α	14.8°	α′	6.1°	α″	12.1°
Complex **6**					
W−S(1)	2.3903(4)	W−S(2)	2.3882(4)	W−S(11)	2.3738(5)
S(1)−C(1)	1.736(2)	S(2)−C(2)	1.738(2)	S(11)−C(11)	1.742(2)
C(1)−C(2)	1.362(3)	C(11)−C(11)′	1.364(4)		
Θ_1	30.3°	Θ_2	30.3°	Θ_3	25.7°
α	3.1°	α′	3.1°	α″	0.0°

[a] Defined in Scheme 3.

C−S single bond and longer than a typical C−C double bond, respectively. Again, it is suggestive of either an $(L_3)^{4-}$ or $(L_3)^{5-\bullet}$ ligand set in this monoanionic species. When compared with the structure of **1**, the C−S bonds are longer and the C−C bonds shorter; however, the most critical point is that these differences are *outside* the 3σ level. Clearly, these structures support a ligand-centered

Scheme 3. (a) Twist angle, Θ, and (b) dithiolene fold angles, α, α′, α″

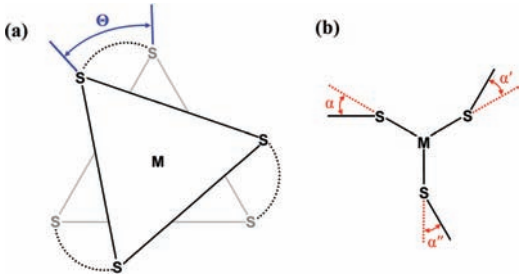

reduction from **1** to **2**. The average Mo−S distance of 2.3734 Å is also longer than observed in **1** at the 3σ level, which may stem from the distorted trigonal prism for **2**.

The structures of neutral molecule in **4**·CH_2Cl_2 and monoanion in **5**·CH_2Cl_2 have been previously solved by Goddard and Holm at 213 K. Though we have repeated these measurements at 100 K with different solvents of crystallization, the metric parameters are virtually identical albeit for marginally improved standard deviations for the low temperature data. An improved data set for $[NEt_4]_2[W(mdt)_3]$ was also obtained (Figure S1). Selected bond distances and angles of **4** and **5** are reported in Table 2, while the structures are displayed in Figure S2. The average C−S bonds at 1.735 and 1.749 Å, and C−C distances of 1.378 and 1.359 Å for **4** and **5**, respectively, are consistent with a ligand-centered redox event; however, the difference in these intraligand distances is within the 3σ level.

The structures of the dianions in **3** and **6** with tetraphenylarsonium countercations solved at room temperature have been reported by Stiefel et al. in 1973.[7,8] We have revisited these complexes with tetraphenylphosphonium cations at 100 K and are able to show the very close similarity between the structures. Selected bond distances and angles are reported in Table 2. A depiction of the dianion in **3** is presented in Figure 2, whereas the corresponding dianion in **6** is shown in Figure S2.

For complexes with $(mnt)^{2-}$ ligands, it is generally regarded that the intraligand bond distances remain constant irrespective of whether oxidized ligands exist in the molecule.[41,42] For instance, the average C−S and C−C bond lengths in $[Ni(mnt)_2]^{1-/2-}$ are essentially identical,[43] despite the monoanion possessing one monoanionic $(mnt)^{1-\bullet}$ ligand.[44] Nevertheless, it is clear that the $[M(mnt)_3]^{2-}$ (M = Mo, W) dianions contain three closed-shell $(mnt)^{2-}$ dithiolate ligands bound to a +IV central ion. The average twist angles are identical with no folding of the dithiolene ligands.

The average twist and dithiolene fold angles for neutral complexes **1** and **4**, and monoanions in **2** and **5**, are compared with $[V(pdt)_3]^{0/1-}$,[42] and $[Re(pdt)_3]^{0}$,[3] in Table 3; the trend in intraligand C−S and C−C bond distances is shown in Figure 3. It has been shown recently that the vanadium species are formulated as $[V^{IV}(L_3^{4-})]^0$ and $[V^{IV}(L_3^{5-\bullet})]^{1-}$, respectively,[42] and the neutral rhenium compound as $[Re^{V}(L_3^{5-\bullet})]^0$.[19] These determinations were elucidated primarily by spectroscopy; however, the short C−S and long C−C bonds are consistent with a specified degree of ligand oxidation. These compounds are therefore useful benchmarks when assessing the oxidation level of the ligands in the neutral and monoanionic molybdenum and tungsten complexes. From the plot shown in Figure 3, a C−S distance of ~1.70 Å indicates an $(L_3)^{4-}$ ligand set and a distance

dx.doi.org/10.1021/ic2006265 |*Inorg. Chem.* 2011, 50, 7106–7122

Table 3. Average Twist (Θ_{av}) and Fold (α_{av}) Angles for Crystallographically Characterized $[M(pdt)_3]^{0/1-}$ (M = V, Mo, W, Re) Complexes

complex	Θ_{av}	α_{av}	ref
$[V(pdt)_3]^0$	4.7°	2.5°	42
$[V(pdt)_3]^{1-}$	0.8°	23.7°	42
$[Mo(pdt)_3]^0$ (**1**)	3.0°	17.4°	this work
$[Mo(pdt)_3]^{1-}$	18.0°	11.0°	this work
$[W(pdt)_3]^0$ (**4**)	3.1°	19.7°	this work
$[W(pdt)_3]^{1-}$	22.8°	11.0°	this work
$[Re(pdt)_3]^0$	3.8°	1.3°	3

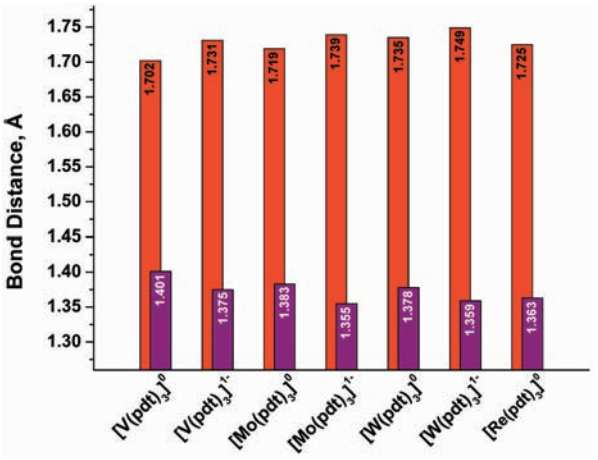

Figure 3. Comparison of intraligand C−S (orange) and C−C (purple) bond distances in crystallographically characterized $[M(pdt)_3]^z$ (M = V, Mo, W, Re; z = 0, 1−).

of ~1.73 Å an $(L_3)^{5-\bullet}$ moiety. The difference of 0.02 Å in the C−S bond distance upon reducing **1** to **2** is outside the 3σ level for the structure resolution and is indicative of ligand-centered reduction. However, the C−S distance of 1.719 Å in **1** falls between 1.70 and 1.73 Å, the values anticipated for two and one oxidative holes, respectively, to the L_3 ligand set. For **2**, the distance at 1.739 Å is more in keeping with an $(L_3)^{5-\bullet}$ ligand set, which is consistent with the EPR and electronic spectra described below and the S K-edge XAS data.[20] On that basis, we are inclined to assume that **1** is formulated as $[Mo^{IV}(L_3^{4-})]^0$, though it could quite possibly be the case that integer oxidation state assignments are not appropriate. Notably, all neutral molybdenum tris(dithiolene) complexes are highly trigonal prismatic with significant dithiolene fold angles (Table S1). In this respect, they are structurally similar to the isoelectronic tris(dithiolene)vanadium monoanions (Table 3) though the latter clearly possess only one ligand oxidative hole.[42] It was postulated that the dithiolene folding, which lowers the point symmetry $D_{3h} \rightarrow C_{3h}$ allowing the singly occupied molecular orbitals (SOMOs) $3a_1'$ (d_{z^2}) and $2a_2'$ to mix because they reduce to a' at lower symmetry, was driven by the strong antiferromagnetic coupling in this singlet diradical. Similar proposals have been advanced for neutral molybdenum tris(dithiolenes), with Campbell and Harris reporting a stabilization of the purely ligand $2a_2'$ orbital over the $3a_1'$ (d_{z^2}) orbital that gives rise to a Mo(VI) oxidation state.[45] Solomon and co-workers reversed that position by stating the opposite occurred, leading to a doubly occupied $3a_1'$ orbital giving a +IV oxidation state that was corroborated by spectroscopic data.[20]

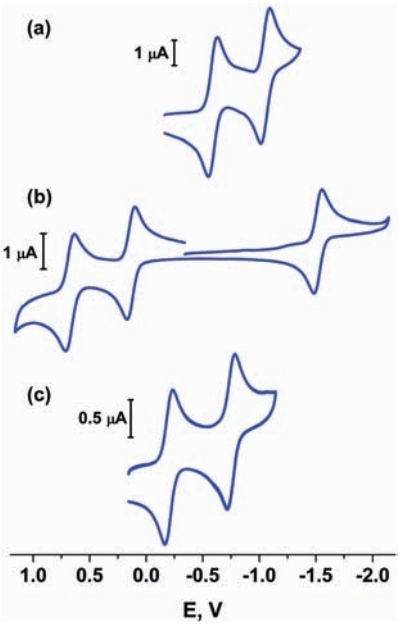

Figure 4. Cyclic voltammograms of (a) $[Mo(pdt)_3]$ (**1**), (b) $[Mo(mnt)_3]^{2-}$ (**3**), and (c) $[Mo(bdt)_3]$ in CH_2Cl_2 solution [0.10 M $[N(n\text{-}Bu)_4]PF_6$ supporting electrolyte at 22 °C at a scan rate of 100 mV s^{-1} (glassy carbon working electrode)]. Potentials are referenced versus the Fc^+/Fc couple.

The neutral complex in crystals of $\mathbf{4}\cdot CH_2Cl_2$ has slightly longer C−S and shorter C−C bond distances than its molybdenum analogue. Moreover, the change in the intraligand bond distances when **4** is reduced by one electron to **5** is within the 2σ level, so it cannot be ascertained from the structure if this event is ligand- or metal-centered. Given the structural similarity to the monoanion in **2**, both in regard to the intraligand bond distances and twist and fold angles, the monoanion in **5** can be formulated as $[W^{IV}(L_3^{5-\bullet})]^{1-}$. Therefore, neutral **4** could be described as $[W^{IV}(L_3^{4-})]^0$ or $[W^{V}(L_3^{5-\bullet})]^0$ since both are consistent with the crystallographic data.

3. Electro- and Spectroelectrochemistry. Cyclic voltammograms of all complexes have been recorded in CH_2Cl_2 solutions containing 0.1 M $[N(n\text{-}Bu)_4]PF_6$ as supporting electrolyte at a glassy-carbon working electrode at ambient temperature. The CVs of **1**, **3**, and $[Mo(bdt)_3]$ are shown in Figure 4, and the potentials referenced versus the ferrocenium/ferrocene couple (Fc^+/Fc) are summarized in Table 4.

The CV of **1** displays two reversible one-electron reductions to its monoanion, $[Mo(pdt)_3]^{1-}$, and dianion, $[Mo(pdt)_3]^{2-}$, and is typical of all neutral complexes. Additionally, an irreversible oxidation (not shown) was also observed in the voltammograms. Among complexes coordinated by type A "olefinic" ligands, the potential corresponding to the 0 → 1− reduction is essentially the same (~-0.60 V) for **1**, $[Mo(sdt)_3]$, and $[Mo(edt)_3]$ (Table 4). However, the potentials for a second reduction to the dianions occur in the order $[Mo(edt)_3]^{1-} < [Mo(pdt)_3]^{1-} < [Mo(sdt)_3]^{1-}$. The relative ordering $[Mo(pdt)_3]^{1-} < [Mo(sdt)_3]^{1-}$ has been observed previously but with a slightly larger difference.[23]

The CV of **3** shows three waves that correspond to one reversible oxidation and one reduction; the second one-electron oxidation is merely quasireversible as judged by controlled

dx.doi.org/10.1021/ic2006265 |Inorg. Chem. 2011, 50, 7106–7122

Table 4. Redox Potentials (V) of Complexes Versus Fc^+/Fc

complex[a]	$E^1_{1/2}$ 1+/0	$E^2_{1/2}$ 0/1−	$E^3_{1/2}$ 1−/2−	$E^4_{1/2}$ 2−/3−	$E^5_{1/2}$ 3−/4−	ref
$[Mo(edt)_3]^0$	+0.94 irr[b]	−0.61 r	−1.12 r			this work
$[Mo(sdt)_3]^0$	+0.85 irr	−0.61 r	−0.99 r			23,46
$[Mo(pdt)_3]^0$	+0.54 irr	−0.60 r	−1.06 r			23,25,47
$[Mo(mnt)_3]^{2-}$		+0.70 qr	−0.15 r	−1.51 r	−2.25 irr	24,47−50
$[Mo(bdt)_3]^0$	+0.93 irr	−0.20 r	−0.75 r			9,25
$[Mo(tbbdt)_3]^0$	+0.91 irr	−0.48 r	−0.99 r			13
$[Mo(qdt)_3]^{1-}$		+0.58 irr	−0.24 r	−1.87 r		5
$[W(mdt)_3]^0$	+0.67 irr	−0.89 r	−1.38 r			12
$[W(pdt)_3]^0$	+0.84 irr	−0.61 r	−1.09 r			23−25,47
$[W(mnt)_3]^{2-}$		+0.61 irr	+0.07 r	−1.80 r	−2.32 irr	24,47,49,50
$[W(bdt)_3]^0$	+1.00 irr	−0.23 r	−0.92 r			25
$[W(tbbdt)_3]^0$	+0.95 irr	−0.47 r	−1.11 r			13

[a] Recorded in CH_2Cl_2 solutions containing 0.1 M $[N(n\text{-}Bu)_4]PF_6$ at 25 °C using a scan rate of 100 mV s^{-1}. [b] r = reversible; qr = quasireversible; irr = irreversible.

potential coulometry. The highly electron withdrawing cyanide groups conjugated with the S_2C_2 dithiolene chelate of the $(mnt)^{2-}$ ligand cause **3** to exhibit the most positive reduction potentials for the type A complexes, and this leads to the appearance of a 3−/4− process at −2.25 V versus Fc^+/Fc. This event is not reversible by coulometry;[49] nonetheless, a ν(CN) stretching frequency of 2134 cm^{-1} was experimentally measured.[48]

Of complexes with type B ligands, the potentials are most negative for $[Mo(tbbdt)_3]$ owing to the electron donating property of the ^{t}Bu groups.[13] The electron withdrawing heteroaromatic $(qdt)^{2-}$ ligand ensures the most positive potentials, with the 1−/2− reduction potential nearly 1 V more positive than the corresponding process in $[Mo(bdt)_3]$. This compound is the only member of its set to have a trianionic species in its electron transfer series, which occurs at −1.87 V. Overall, the complexes with the olefinic dithiolene ligands other than $(mnt)^{2-}$ (type A) are more easily oxidized than their counterparts with aromatic dithiolene ligands (type B).

The potentials of the first reduction processes for the corresponding tungsten tris(dithiolene) complexes are essentially the same as their molybdenum analogues and underscore the ligand-centered nature of these redox events. The second reduction occurs at slightly lower potentials, which stems from the more pronounced relativistic effects for 5d than 4d orbitals.[51] Comparative potentials of Mo and W complexes bearing dithiolene ligands have been listed elsewhere.[52] Unlike **3**, the 0/1− process of **6** is irreversible. However, it does share reversible 1−/2− and 2−/3− couples with its Mo analogue. The 3−/4− couple is also irreversible by coulometry.

Since the redox potentials are well separated from each other, we performed controlled potential electrolysis experiments to examine the reversibility of the redox processes and isolate reduced and oxidized forms of the transfer series and record their electronic absorption spectra. The spectra of the three-membered series for **1** (top) and $[Mo(bdt)_3]$ (bottom) are shown in Figure 5. Key absorption maxima and extinction coefficients are collated in Table 5.

The electronic spectra for all neutral compounds have a characteristically intense band in the 600−700 nm region with an extinction coefficient ranging $1-6 \times 10^4$ M^{-1} cm^{-1}. Given its significant intensity, which is not only dependent on the ligand type, A or B, but also on the dithiolene or aromatic

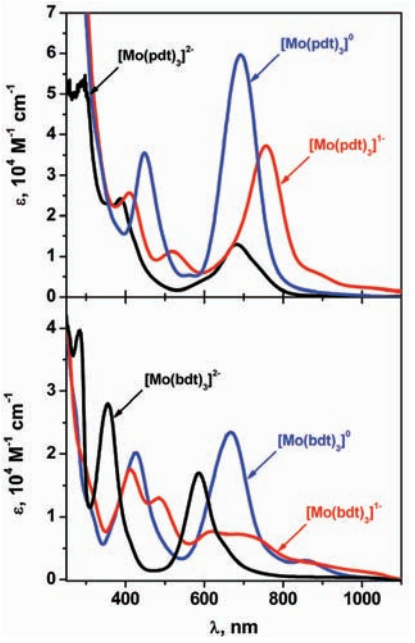

Figure 5. Electronic spectra of electrochemically generated neutral (blue), monoanionic (red), and dianionic (black) $[Mo(pdt)_3]^z$ (z = 0, 1−, 2−) species (top) and $[Mo(bdt)_3]^z$ (0, 1−, 2−) (bottom) in CH_2Cl_2 (0.10 M $[N(n\text{-}Bu)_4]PF_6$) at −25 °C.

dithiolate substituents, this band is tentatively assigned as a ligand-to-ligand charge transfer (LLCT) band that is the fingerprint for an oxidized ligand set, either $(L_3)^{4-}$ or $(L_3)^{5-\bullet}$. Since all neutral compounds exhibit this band, we can exclude the possibility of a +VI central ion in these complexes, though whether there is a +IV or +V central ion cannot be discriminated by electronic spectroscopy. A second intense band at around 400 nm is evident in all spectra. Additionally, complexes with type B ligands reveal a weakly intense shoulder in the near-IR region (762−881 nm).

A very clear difference is witnessed when comparing the electronic spectra of the monoanionic complexes with type A and B ligands. As shown in Figure 6, these complexes give rise to distinctly different spectral profiles with type A ligands showing

dx.doi.org/10.1021/ic2006265 |Inorg. Chem. 2011, 50, 7106–7122

Table 5. Salient Absorption Bands [λ_{max}, nm (ε, 10^4 M^{-1} cm^{-1})] in Electronic Spectra of Electrochemically Generated Species in CH_2Cl_2 Solutions Containing 0.1 M $[N(n\text{-}Bu)_4]PF_6$, at −25 °C

M	ligand	neutral	monoanion	dianion	trianion
Mo	edt	602 (1.15), 412 (1.03)	999 (0.06), 687 (0.59)	673 (0.52), 378 (0.59)	
Mo	sdt	668 (1.54), 443 (1.11)	1008 (0.07), 747 (0.88)	686 (0.61), 400 (1.15)	
Mo	pdt	691 (5.97), 447 (3.55)	990 (sh, 0.24), 756 (3.73)	682 (1.29), 338 (2.42)	
Mo	mnt		964 (0.10), 692 (1.03)	669 (0.66), 390 (1.05)	961 (0.18), 563 (1.23)
Mo	bdt	855 (0.30), 667 (2.34), 426 (2.01)	836 (sh, 0.30), 679 (0.72), 621 (0.77)	585 (1.69), 355 (2.81)	
Mo	tbbdt[a]	881 (0.32), 667 (2.34), 426 (2.01)	862 (sh, 0.23), 701 (0.80), 638 (0.88)	575 (1.71), 353 (2.01)	
Mo	qdt		782 (sh, 0.60), 697 (1.19), 613 (1.54)	563 (5.22), 397 (4.32)	760 (0.57), 563 (1.10)
W	mdt	608 (1.76), 401 (0.94)	915 (0.07), 671 (0.69)	617 (0.35), 524 (0.67)	
W	pdt	657 (3.12), 414 (1.39)	901 (0.10), 687 (1.54)	616 (0.53), 525 (0.88)	
W	mnt		900 (0.03), 618 (0.63)	571 (0.43), 491 (0.33)	1033 (0.25), 528 (0.96)
W	bdt	762 (0.20), 623 (1.72), 381 (1.26)	639 (sh, 0.08), 568 (sh, 0.50)	548 (0.57), 475 (1.46)	
W	tbbdt[a]	790 (0.35), 649 (2.53), 390 (1.90)	632 (0.61), 537 (1.17)	539 (0.90), 468 (2.45)	

[a] Data taken from ref 13.

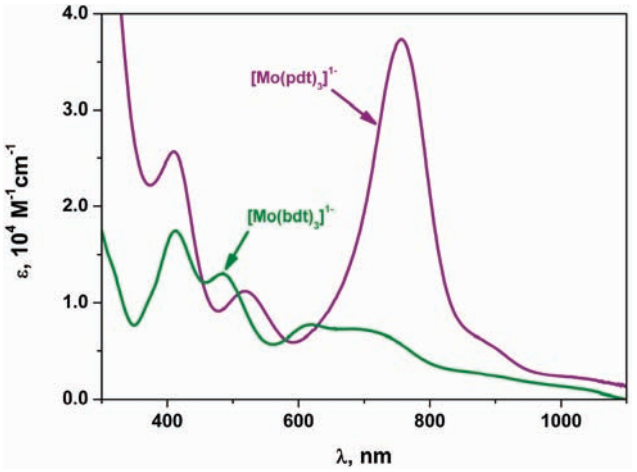

Figure 6. Overlay of the electronic spectra of $[Mo(pdt)_3]^{1-}$ (purple) and $[Mo(bdt)_3]^{1-}$ (green) in CH_2Cl_2 (0.10 M $[N(n\text{-}Bu)_4]PF_6$) at −25 °C.

an intense asymmetric band in the range 687−756 nm. This can be interpreted as a LLCT band in these systems, and more importantly, the intensity is approximately half that for the same transition in the corresponding neutral species. This could be evidence of a $[M^{IV}(L_3^{5-\bullet})]^{1-}$ formulation for these type A complexes, which is in keeping with the EPR and X-ray crystallography. On the other hand, type B ligands possess 2−3 weak to moderately intense bands >600 nm that are purported as evidence for a fully reduced ligand set, $(L_3)^{6-}$. Moreover, complexes with type A ligands show an additional transition in the near-IR region, from 900 to 1000 nm.

The dianionic members of these series display two prominent bands in their absorption spectra. For molybdenum with type A ligands, these bands are in the ranges 669−686 and 338−400 nm, respectively. The aromatic dithiolate ligated complexes are at slightly higher energies of 563−585 and 353−397 nm, respectively. The tungsten analogues show the same profile, albeit at slightly different wavelengths. Due to the presence of three dianionic dithiolate ligands, $(L_3)^{6-}$, these intense features are ligand-to-metal charge transfer (LMCT) bands to empty Mo and W d orbitals with significant sulfur 3p character. The three trianionic species are characterized by one prominent LMCT band at 528 (for W) or 563 nm (for Mo), and a NIR band of moderate intensity (Figures S7, S8, and S11).

4. CALCULATIONS

a. Geometries. Table 6 presents the calculated metric parameters for the geometry optimized structures of $[Mo(bdt)_3]^{1-}$, $[Mo(edt)_3]^{1-}$, $[W(bdt)_3]^{1-}$, and $[W(mdt)_3]^{1-}$, and a comparison with experimental data.[12,15,53] For $[Mo(edt)_3]^{1-}$, in the absence of a crystal structure, we have used the metric data for $[NEt_4]$-$[Mo(mdt)_3]$ given the reasonable similarity in the dithiolene ligand substitution.[14] For $[M(bdt)_3]^{1-}$ (M = Mo, W), there is an excellent agreement with the experimental findings, with only a slight overestimation of the M−S bond distances typical for present day functionals. The intraligand C−S bond lengths of 1.754 and 1.757 Å, respectively, and the arithmetic average aromatic C−C distances are indicative of three closed-shell $(bdt)^{2-}$ ligands bound to the central M(V) ion: $[M^V(^BL_3^{6-})]^{1-}$ (M = Mo, W). The computed twist angles of 33.2° (for $[Mo(bdt)_3]^{1-}$) and 32.9° (for $[W(bdt)_3]^{1-}$) match nicely with the crystallographic distortion toward the octahedral limit for complexes of this type.[8,54,55] The calculated fold angles are nearly zero, and therefore the experimental values of 9.9° and 2.8°, respectively, are plausibly attributed to lattice packing effects.

The geometry optimized structure of $[Mo(edt)_3]^{1-}$ exhibits a perfectly trigonal prismatic MoS_6 core, with the average twist angle Θ_{av} = 0.2°.[8,55] The intraligand C−S and C−C bond distances of 1.723 and 1.353 Å, respectively, very reasonably match the experimental data; the short C−S and long olefinic C−C distances suggest an $(L_3)^{5-\bullet}$ redox level to the tris(dithiolene) unit bound to a Mo(IV) d^2 central ion.

There is noticeable disagreement in the optimized C−S bond distance of 1.754 Å and the crystallographic average of 1.730(10) Å[12] for $[W(mdt)_3]^{1-}$. While the computed value is within the 3σ confidence limit due to the low resolution of the crystal structure, a similar distance of 1.726(8) Å in $[Mo(mdt)_3]^{1-}$ suggests that the optimized structure has more reduced dithiolene ligands than the solid state structure.[14] This difference stems from the very pronounced dithiolene fold in the optimized structure for $[W(mdt)_3]^{1-}$, with α_{av} = 14.6° twice as large as found in the crystal structure. It was established in a recent study on analogous $[V(dithiolene)_3]^{1-}$ complexes[42] that crystal packing can easily account for the small energetic difference (<3 kcal mol^{-1}) between flat and folded tris(dithiolene) conformations. Irrespective of the ligand substituents (for type A dithiolene ligands, Scheme 1) or functional used, we consistently found the dithiolene-folded

dx.doi.org/10.1021/ic2006265 |Inorg. Chem. 2011, 50, 7106–7122

Table 6. Average Calculated (DFT) and Experimental (Crystallography) Metric Parameters

	$[Mo(bdt)_3]^{1-}$		$[Mo(edt)_3]^{1-}$		$[W(bdt)_3]^{1-}$		$[W(mdt)_3]^{1-}$	
	exptl[a]	calcd	exptl[b]	calcd	exptl[c]	calcd	exptl[d]	calcd
M−S (Å)	2.386	2.415	2.374(2)	2.416	2.37(1)	2.412	2.375(2)	2.407
S−C (Å)	1.749	1.754	1.726(8)	1.723	1.71(4)	1.757	1.73(1)	1.754
C−C[e] (Å)			1.35(1)	1.353			1.35(1)	1.353
$C_{arom}-C_{arom}$[f] (Å)	1.390	1.396			1.41(6)	1.396		
SMS_{intra}[g] (deg)	81.9	81.7	81.5	81.6	81.8	81.8	80.4	79.5
α[h] (deg)	9.2	1.1	4.0	0.8	2.8	0.5	7.2	14.6
Θ[h] (deg)	35.2	33.2	1.6	0.2	32.3	32.9	2.9	1.1

[a] Structure from ref 15. [b] Structure of $[NEt_4][Mo(mdt)_3]$ from ref 14. [c] Structure from ref 53. [d] Structure from ref 12. [e] Dithiolene carbon atoms. [f] Arithmetic average C−C bond distance of the aromatic ring. [g] S−M−S intraligand bite angle. [h] Defined in Scheme 3.

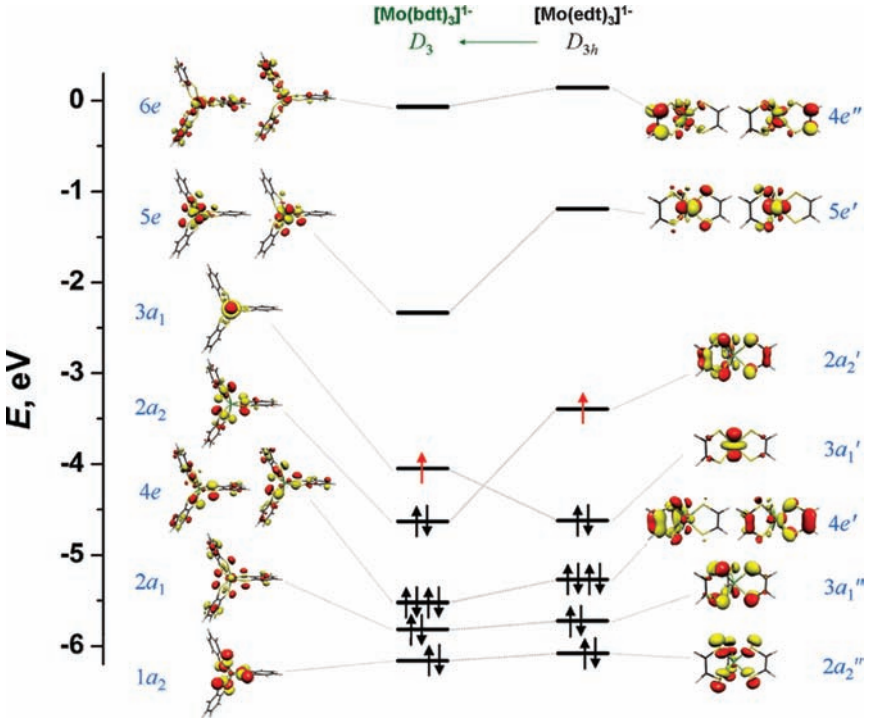

Figure 7. Molecular orbital scheme for $[Mo(bdt)_3]^{1-}$ (D_3 symmetry labels, left) with type B ligands and $[Mo(edt)_3]^{1-}$ (D_{3h} symmetry labels, right) with type A ligands showing frontier canonical orbitals derived from ZORA/B3LYP DFT calculations.

C_{3h} structure preferred over the higher symmetry D_{3h} one.[56] In the absence of lattice packing forces, an electronic effect appears to be operative in the tungsten complexes that is not exerted in the analogous molybdenum compounds. Although the point is outside the scope of the present study, the origin of this difference between $[Mo(mdt)_3]^{1-}$ and $[W(mdt)_3]^{1-}$ warrants deeper scrutiny. Despite the different values for α, both the calculated and experimental WS_6 cores are highly trigonal prismatic with negligible twist angles.

b. Electronic Structure. For the MO description of these tris(dithiolene) complexes, we choose the 3-fold axis as the *z*-axis; the *x*-axis bisects one of the dithiolene ligands. The qualitative bonding scheme for $[Mo(bdt)_3]^{1-}$ and $[Mo(edt)_3]^{1-}$ derived from spin-unrestricted B3LYP DFT calculations is shown in Figure 7. Considering the higher symmetry ion, that of $[Mo(edt)_3]^{1-}$ within the D_{3h} point group, the ligand field splitting of d orbitals gives a_1' (d_{z^2}), e' ($d_{x^2-y^2,xy}$), and e'' ($d_{xz,yz}$) levels. Similarly, there are sets of σ orbitals of the tris(dithiolene) unit which have the appropriate symmetry to interact with each of the metal d orbitals, as well as π combinations that interact with the metal e' and e'' orbitals. Additionally, two ligand π orbitals are nonbonding with respect to the metal, namely the a_2' and a_2'' orbitals.[19,25,42,45] This generates a complicated interaction picture between what is classified as a two-center arrangement between the metal and the tris(dithiolene) unit, L_3. Stiefel et al. summarized the four typical interactions as:[25] (1) σ bonding between ligand σ orbitals that point toward the metal d_{xz} and d_{yz} orbitals; (2) bonding between ligand σ orbitals and the metal d_{z^2} orbital, described as a combination of σ and π interactions; (3) donation from ligand π orbitals orthogonal to the ligand plane into metal $d_{x^2-y^2}$ and d_{xy} orbitals; and (4) donation from these same ligand π orbitals into the metal d_{xz} and d_{yz} orbitals that generate π- and δ-type interactions.

dx.doi.org/10.1021/ic2006265 |*Inorg. Chem.* 2011, 50, 7106–7122

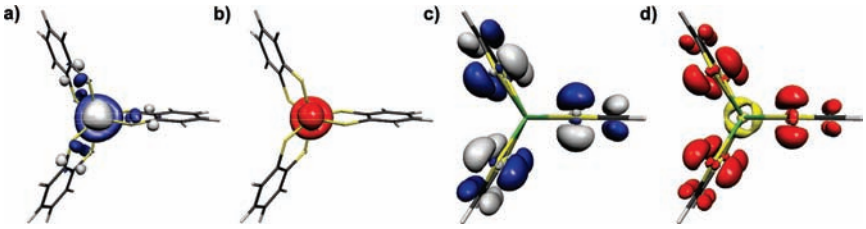

Figure 8. Isosurface plots of (a) the ground state molecular orbital of $[Mo(bdt)_3]^{1-}$, (b) Mulliken spin density map for $[Mo(bdt)_3]^{1-}$, (c) the ground state molecular orbital of $[Mo(edt)_3]^{1-}$, and (d) Mulliken spin density map for $[Mo(edt)_3]^{1-}$, derived from ZORA/B3LYP DFT calculations and viewed along the C_3 axis (red, α-spin; yellow, β-spin).

Table 7. Isotropic and Anisotropic *g*- and *A*-values ($\times 10^{-4}$ cm^{-1}) for Complexes Derived from Simulation of Chilled (200 K) and Frozen Solution (30 K) Multifrequency EPR Spectra

complex	g_{iso}	A_{iso}	g_x	g_y	g_z	$\langle g\rangle^a$	Δg^b	A_x	A_y	A_z	$\langle A\rangle^c$
					L^A						
$[Mo(edt)_3]^{1-}$	2.0106	12.6	2.0095	2.0099	2.0124	2.0106	0.0029	9	17	14.5	13.5
$[Mo(sdt)_3]^{1-}$	2.0101	11.6	2.0110	2.0119	2.0121	2.0117	0.0011	12	15	11	12.7
$[Mo(pdt)_3]^{1-}$	2.0125	9.4	2.0120	2.0121	2.0156	2.0132	0.0036	6	12.5	10	9.5
$[Mo(mnt)_3]^{1-d}$	2.0108	11.8	2.0107	2.0109	2.0132	2.0116	0.0025	8	16	13	12.3
					L^B						
$[Mo(bdt)_3]^{1-}$	2.0061	27.1	2.0207	2.0076	1.9944	2.0076	0.0263	39	29	13	27.0
$[Mo(tbdt)_3]^{1-}$	2.0050	24.6	2.0203	2.0081	1.9955	2.0080	0.0248	39	24	13	25.3
$[Mo(qdt)_3]^{1-}$	2.0004	28.7	2.0123	2.0059	1.9930	2.0037	0.0193	39	40	7	28.7
					L^A						
$[W(mdt)_3]^{1-}$	1.9941	−27.3	2.0094	2.0012	1.9878	1.9995	0.0216	−32	−34	−11	−25.7
$[W(pdt)_3]^{1-}$	1.9933	−27.0	2.0075	2.0018	1.9907	2.0000	0.0168	−30	−31	−12	−24.3
$[W(mnt)_3]^{1-d}$	1.9946	−29.4	1.9864	1.9896	2.0006	1.9922	0.0142	−18	−34	−32	−28.0
					L^B						
$[W(bdt)_3]^{1-}$	1.9825	−48.0	2.0237	2.0069	1.9448	1.9918	0.0789	−59	−70	−26	−51.7

$^a \langle g\rangle = {}^1/_3(g_x + g_y + g_z)$. ^{b} Anisotropy, $\Delta g = g_x - g_z$. $^c \langle A\rangle = {}^1/_3(A_x + A_y + A_z)$. ^{d} Sample generated by controlled potential coulometry under conditions specified in the Experimental Section.

The correct energetic ordering of these frontier orbitals is key to diagnosing the correct electronic structure.[19,20,42] For $[Mo(edt)_3]^{1-}$, the electronic structure described as $[Mo^{IV}(^AL_3^{5-\bullet})]^{1-}$ bears the electron configuration $(4e')^4(3a_1')^2(2a_2')^1(5e')^0$; the $2a_2'$ SOMO (Figure 8c) is consistent with the EPR data (vide infra), as well as the results from the recent S K-edge XAS and DFT study by Solomon and co-workers.[20] Here, the π donor strength of the $(edt)^{2-}$ ligand destabilizes the $2a_2'$ MO with respect to the metal-centered $3a_1'$ MO, and the trigonal prismatic structure prevails despite the SOMO being antibonding with respect to this geometry. Substituting the olefinic tris(dithiolene) system (type A, Scheme 1) for an aromatic one (type B, Scheme 1) demonstrates the participation of the conjugation pathways that attenuate π donor strength in type B ligands. Here, the significant trigonal twist angle represents a downgrading of symmetry from D_{3h} to D_3 that is driven by a configurational interaction between the predominantly metal $3a_1'$ and ligand $3a_1''$ MOs ($3a_1$ and $2a_1$ in Figure 7) which stabilize a distorted octahedron. Additionally, the $2a_2'$ MO is stabilized with respect to the $3a_1'$ through decreased interligand repulsion as the distance between S-donor atoms increases upon twisting. This electronic effect was the salient point elegantly detailed by Solomon and co-workers.[20] Therefore, the resultant electron configuration of $(4e)^4(2a_2)^2(3a_1)^1(5e)^0$ gives rise to a $[Mo^V(^BL_3^{6-})]^{1-}$ formulation for $[Mo(bdt)_3]^{1-}$, and all other complexes bearing type B ligands have a metal-centered $3a_1$ ground state as depicted in Figure 8a. This different electronic structure is clearly evident in the *g*-anisotropy, which is considerably larger for type B ligand systems owing to more efficient spin−orbit coupled excited state admixtures with the metal-centered ground state (vide supra). The preference for a distorted octahedral structure for $[Mo(^BL_3)]^{1-}$ arises from the small splitting between the $3a_1'$ and $3a_1''$ MOs inherent to aromatic-1,2-dithiolenes.

The MO manifold for analogous tungsten complexes is presented in Figure S13. The middle scheme is the bonding arrangement for trigonal prismatic $[W(mdt)_3]^{1-}$, computed on crystal structure coordinates. The small splitting of what are essentially degenerate *e* levels stems from minor distortions of the solid state structure that slightly perturbs this degeneracy. Naturally, the optimized structures of $[W(bdt)_3]^{1-}$ (Figure S13, left) and $[W(mdt)_3]^{1-}$ (Figure S13, right) exhibit no such distortions. Nevertheless, the D_{3h} structure is a useful starting point to assess the effect of ligand folding (Scheme 3) that is a lowering of point symmetry to C_{3h}. As mentioned previously, the $[W(^AL_3)]^{1-}$ complexes consistently optimized with a C_{3h} structure: even $[W(pdt)_3]^{1-}$ adopts this conformation which is far removed from its crystallographic distorted trigonal prismatic structure ($\Theta_{av} = 22.8°$). Ligand folding was first investigated by

dx.doi.org/10.1021/ic2006265 |*Inorg. Chem.* 2011, 50, 7106–7122

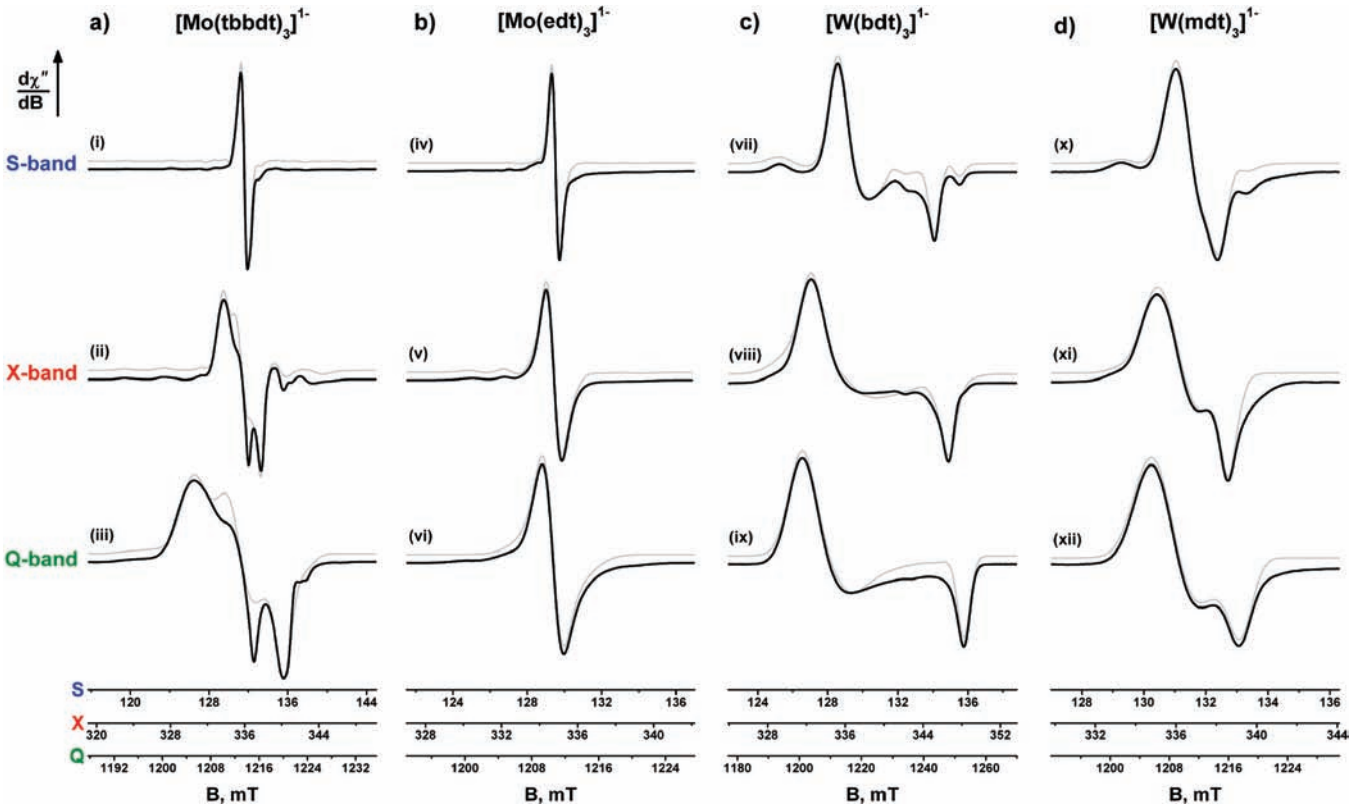

Figure 9. Multifrequency EPR spectra of (a) $[Mo(tbbdt)_3]^{1-}$, (b) $[Mo(edt)_3]^{1-}$, (c) $[W(bdt)_3]^{1-}$, and (d) $[W(mdt)_3]^{1-}$, recorded at S-, X-, and Q-band frequencies, respectively. Experimental spectra measured at 30 K are shown as black lines and simulations depicted by the gray trace. Experimental conditions are listed in Tables S7−S9 in the Supporting Information.

Campbell and Harris,[45] who determined the effect results from a second-order Jahn−Teller distortion brought about by the small HOMO−LUMO ($3a_1'$ and $2a_2'$ MOs, respectively) energy gap in neutral tris(dithiolene)molybdenum complexes. The distortion leads to a stabilization of the HOMO, which was correctly identified as the d_{z^2} orbital by Solomon and co-workers.[20] At this stage we cannot account for this disparity between geometry optimized and solid structures for $[W(mdt)_3]^{1-}$, though it may simply be the case that the C_{3h} structure is the most stable in solution whereas the demands of crystal packing lead to the higher symmetry orientation. Alas, EPR data are not irrefutable proof that this calculated electronic structure is true, and additional input ideally from S K-edge XAS analysis of both the solid and solution samples appears necessary to validate this computational result.

5. EPR SPECTROSCOPY

a. Isotropic Spectra. Fluid solution S- and X-band EPR spectra of the complexes in dichloromethane or THF were recorded at 200 K. The advantage of the chilled temperature is reduction of the intrinsic field-dependent linewidth and enhancement of the signal intensity and the spectral resolution. For the molybdenum complexes, the spectra exhibit one central resonance from naturally occurring isotopes with no nuclear spin (^{90,92,94,96,98,100}Mo, 74.53% abundant) flanked by six hyperfine resonances from the ^{95,97}Mo ($I = {}^5/_2$, 25.47% natural abundance) isotopes. The tris(dithiolene)tungsten monoanions displayed a broad, featureless resonance at X-band where the hyperfine satellites from the ^{183}W ($I = {}^1/_2$, 14.31% natural abundance) isotope are buried in the spectral linewidth. The prudent use of S-band frequencies (~3.7 GHz) and chilled temperatures resolved these hyperfine features. Computer simulation of these spectra afforded isotropic g-values and metal hyperfine coupling constants that are posted in Table 7. The average isotropic g-value for $[Mo(^AL_3^{5-\bullet})]^{1-}$ complexes at $g_{iso} = 2.011$ is noticeably higher than that for $[Mo(^BL_3^{6-})]^{1-}$ at $g_{iso} = 2.004$. However, the hyperfine coupling constants are markedly different between the two types of complexes, where ^{A}L containing species have $A_{iso} \sim 10 \times 10^{-4}$ cm^{-1} compared to those with ^{B}L ligands at $A_{iso} \sim 25 \times 10^{-4}$ cm^{-1}, and are crucial in evaluating the relative sign of the principal A-values in anisotropic spectra. A similar pattern is observed with the analogous tungsten species, though the g-values are lower because of the very large spin−orbit coupling constant for the third-row metal, $\xi_W = 2700$ cm^{-1} (cf. $\xi_{Mo} = 900$ cm^{-1}, vide infra).[57] For the two different isomers of asymmetric complexes $[Mo(sdt)_3]^{1-}$ and $[Mo(tbbdt)_3]^{1-}$, the differences in their respective spin-Hamiltonian parameters are not large enough to be distinguished in the fluid solution spectra, nor the frozen solution spectra, though they contribute to the experimental linewidths. The W complexes yield much larger isotropic hyperfine coupling constants with values ranging $27.0-29.4 \times 10^{-4}$ cm^{-1}, which are dwarfed by $A_{iso} = 48 \times 10^{-4}$ cm^{-1} of $[W(bdt)_3]^{1-}$. There is a clear difference in the location of the unpaired spin in these tris(dithiolene) monoanions as demonstrated by the fluid solution spectra that wholly supported the ground state distinction revealed by S K-edge XAS. Curiously, the fluid solution EPR spectrum of $[Mo^V(abt)_3]^{1-}$

where abt = aminobenzenethiolate(2−) has been reported.[58] Here, with an *N,S*-coordinating ligand, the ^{95,97}Mo hyperfine coupling constant is $\sim 40 \times 10^{-4}$ cm^{-1}. The paramagnetic monoanions derived from one-electron chemical reduction of Mo(tbabt)$_3$ (tbadt = 4,6-di-*tert*-butyl-2-aminobenzenethiolate-(2−)) and Mo(tbcat)$_3$ (tbcat = 3,5-di-*tert*-butylcatecholate-(2−)) displayed hyperfine couplings of 47×10^{-4} cm^{-1} and 50×10^{-4}, respectively,[59] which are approximately twice the value for ^{B}L systems. This is quite a compelling effect on the covalency and reveals that the "Mo(V)" ion in $[Mo^{V}(^{B}L_3^{6-})]^{1-}$ is quite unique, and we assign an integer oxidation state with some trepidation.

b. Anisotropic Spectra. Frozen solution EPR spectra were recorded at S-band (~3.7 GHz), X-band (~9.5 GHz), and Q-band (~34 GHz) frequencies with the intent of retrieving more accurate spin-Hamiltonian parameters. While Q-band EPR spectra provide superior *g*-value resolution, the S-band spectra are most sensitive to metal hyperfine interactions due to enhanced second-order effects on the resonant field positions and reduced *g*−*A* strain which generate narrower linewidths. Anisotropic EPR spectra for $[Mo(tbbdt)_3]^{1-}$, $[Mo(edt)_3]^{1-}$, $[W(bdt)_3]^{1-}$, and $[W(mdt)_3]^{1-}$ together with their simulations are displayed in Figure 9.

Type B Ligands. Complexes with type B ligands, aromatic-1,2-dithiolenes, exhibit anisotropic EPR spectra at cryogenic temperatures. An axial *g*-splitting is expected for a paramagnetic species with the electronic configuration $(d_{z^2})^1$ ground state (Figure 8a), with g_z effectively parallel to the molecular *z*-axis (C_3 symmetry axis).[18] There is an observed splitting of the $g_\perp$ components brought about by a combination of d-orbital mixing into the ground state and CT contributions from the tris(dithiolene) unit. Each spectrum reveals a distinct broadening of g_y due to rampant *g*-strain. This form of line broadening arises from heterogeneity of the molecular structure in the frozen solution matrix; large variation of g_y is a direct response to quite small geometric distortions. The terminal *g*-values ($g_{x,z}$) also experience *g*-strain, though to a much lesser extent, and are therefore more reliably reproduced by simulation. At Q-band frequencies, *g*-strain is more pervasive and we met with varying success in computer simulation of the higher frequency spectra. Using a Gaussian distribution of *g*-values for $[M(^{B}L_3^{5-\bullet})]^{1-}$ (M = Mo, W), satisfactory simulations of the X- and Q-band spectra of $[W(bdt)_3]^{1-}$ (Figure 9c) and $[Mo(qdt)_3]^{1-}$ (Figure S29) were obtained. However, the unusual line shape in X- and Q-band spectra of $[Mo(bdt)_3]^{1-}$ (Figure S28) and $[Mo(tbbdt)_3]^{1-}$ (Figure 9a) produced only mediocre simulations; in fact, the Q-band spectrum of $[Mo(bdt)_3]^{1-}$ could not be simulated. Attempts to modify the spectral profile by altering the concentration, countercations, and glassing conditions failed to alleviate the *g*-strain, which appears to be inherent to this class of compounds. As a result, there is more disparity between the average *g*- and *A*-values compared to the isotropic ones (Table 7).

On the whole, a $g_x > g_y > g_e > g_z$ pattern is identified for all $[M(^{B}L_3^{5-\bullet})]^{1-}$ (M = Mo, W) spectra. The *g*-anisotropy is three times larger for W than Mo in line with the aforementioned spin−orbit coupling constants for these third- and second-row transition metals, respectively. The *A*-splitting is axial with $A_x \approx A_y > A_z$, where the parallel component is approximately half the perpendicular values. Deviation in equivalent A_x- and A_y-values indicates structural distortions about a C_2 axis orthogonal to the main symmetry axis. A recent study of isoelectronic $[V(dithiolene)_3]^{2-}$,[42] also possessing a $(d_{z^2})^1$ ground state, revealed the opposite *g*-splitting: A more axial arrangement with $g_z > g_{x,y}$, and all smaller than g_e. This assignment followed from a single crystal EPR study of $[AsPh_4]_2[V(mnt)_3]$.[18] The hyperfine was also axial, with $A_x \approx A_y \gg A_z$, though the $A_\perp$ values are 2 orders of magnitude larger than A_z. This highlights a greater covalency in the Mo/W−S bonds than V, which distributes more spin density on the ligand framework in the former. The V complexes were diagnosed with polarized V−S bonds that amplified the α-spin density on the metal ion to ~1.4 spins.[42] In contrast, a Mulliken spin population analysis of $[Mo(bdt)_3]^{1-}$ and $[W(bdt)_3]^{1-}$ (Table 8) sees ≤1 spins at the metal ion, consistent with more covalent M−S bonds and a smaller magnetic hyperfine interaction.

Table 8. SOMO Composition (%) and Mulliken Spin Population Analysis for Selected Complexes

			% composition					Mulliken population		
	symmetry	SOMO	M d	M s	S p	C p[a]		M	S	C[a]
$[Mo(bdt)_3]^{1-}$	D_3	$3a_1$	68.5	0.2	12.2	3.6		+1.01	−0.09	+0.05
$[Mo(edt)_3]^{1-}$	D_{3h}	$2a_2'$	0.1	0.0	66.4	22.8		−0.18	+0.94	+0.32
$[W(bdt)_3]^{1-}$	D_3	$3a_1$	63.9	0.1	12.1	4.4		+0.87	+0.01	+0.08
$[W(mdt)_3]^{1-}$	C_{3h}	$4a'$	36.0	0.3	33.4	13.7		+0.45	+0.38	+0.16

[a] Metallodithiolene carbon atoms only.

The variation in *g*-values shown in Table 7 reflects the orbital composition of the electronic ground and excited states, including the degree of metal−ligand covalency, configurational mixing, and metal and ligand spin−orbit coupling. The spin−orbit interaction leads to small admixtures of excited states into the ground state, which in turn shifts the *g*-values away from g_e (= 2.0023) as outlined in eq 1, where ΔE_k is the excitation energy associated with each d−d and CT transition. The terms F_k, G_k, and H_k depend on the composition of the molecular orbitals in the ground and excited states, and include ligand and metal spin−orbit coupling contributions.[60]

$$g_i = \Delta g_i \delta_i + \Delta g_i^{d-d} + \Delta g_i^{MLCT} + \Delta g_i^{LMCT}$$
$$= 2.0023\delta_i - \sum_k \frac{F_k}{|\Delta E_k^{d-d}|} - \sum_k \frac{G_k}{|\Delta E_k^{MLCT}|} + \sum_k \frac{H_k}{|\Delta E_k^{LMCT}|} \quad (1)$$

Therefore, d−d and metal-to-ligand charge transfer (MLCT) transitions lower *g*-values whereas LMCT excitations serve to increase them; the magnitude of the *g*-shifts are inversely proportional to the energy separation between ground and excited states, and can be correlated to changes in electronic absorption spectra.[61] A simple crystal field description of a d^1 ion in a trigonal environment (D_3 symmetry, Figure 7) gives rise to metal-based antibonding wavefunctions shown in eq 2, expressed as linear combinations of the usual d functions in octahedral symmetry.

$$\psi_{z^2}^{a_1*} = \alpha[d_{z^2}]$$
$$\psi_{x^2-y^2}^{5e*} = \beta[\sqrt{2/3}\, d_{x^2-y^2} - \sqrt{1/3}\, d_{yz}]$$
$$\psi_{xy}^{5e*} = \gamma[\sqrt{2/3}\, d_{xy} + \sqrt{1/3}\, d_{xz}]$$
$$\psi_{xz}^{6e*} = \delta[-\sqrt{2/3}\, d_{xz} + \sqrt{1/3}\, d_{xy}]$$
$$\psi_{yz}^{6e*} = \varepsilon[\sqrt{2/3}\, d_{yz} - \sqrt{1/3}\, d_{x^2-y^2}] \quad (2)$$

dx.doi.org/10.1021/ic2006265 |*Inorg. Chem.* 2011, 50, 7106–7122

Here, covalency is accounted for in the orbital coefficients $\alpha, \beta, \gamma, \delta$, and ε; the individual d orbital contributions to each metal-based wavefunction are fixed in strict adherence to the D_3 symmetry of $[M(^{B}L_3^{5-\bullet})]^{1-}$ (M = Mo, W) complexes.[62] Any distortions along a perpendicular C_2 axis will lower the symmetry and lift the excited state degeneracy, thereby altering the d orbital contributions to the ground and excited states of the wavefunctions listed above. Excluding the CT components, incorporation of these metal-based wavefunctions into eq 1 gives the spin−orbit coupling (d−d) derived expressions for the g-shifts (eq 3), where ξ_M is the single electron spin−orbit coupling constant, and $\Delta E_i = |E(\Psi_i) - E(\Psi_{z^2}^{a_1^*})|$ ($i = x^2 - y^2, xy, xz, yz$).

$$g_z = g_e$$

$$g_x = g_e - \frac{4\xi_M\alpha^2\varepsilon^2}{\Delta E_{yz}} - \frac{2\xi_M\alpha^2\beta^2}{\Delta E_{x^2-y^2}}$$

$$g_y = g_e - \frac{4\xi_M\alpha^2\delta^2}{\Delta E_{xz}} - \frac{2\xi_M\alpha^2\gamma^2}{\Delta E_{xy}} \qquad (3)$$

Spin−orbit coupled mixing occurs between the d_{z^2} ground state and excited states with $d_{xz,yz}$ character. Overall, the negative shift supplied by d-d excitations will be small because the dominant contribution from the $3a_1 \rightarrow 6e$ transition is superseded by the very large energy gap between these two states; the contribution is presumably greater from the $5e$ MOs, though these have only 33% contribution from the $d_{xz,yz}$ orbitals (eq 2). It is clear that if d−d transitions from the SOMO to metal-based excited states were dominant in these complexes, a completely different g-splitting would be observed, namely $g_z \approx g_e > g_{x,y}$, which is at odds with the experimental data, especially considering $g_{x,y} > g_e$. Therefore, it is apparent that LMCT transitions from filled ligand orbitals to the ground state that make positive shifts to the g-values are overriding the negative contributions from d−d and MLCT excitations (eq 1). The electronic spectra are replete with intense, low-energy LMCT bands, though the extent of the shift appears to be dependent on spin−orbit coupling; otherwise, the isoelectronic vanadium dianions would experience similarly high $g_{x,y}$ values concomitant with similar low-energy LMCT bands. The lowering of g_z may logically stem from the $3a_1 \rightarrow 5e$ transition since it is endowed with MLCT character owing to the experimentally determined ~50% ligand content of the $5e$ MOs.[20] The energetic difference estimated from the S K-edge spectrum of $[Mo(tbbdt)_3]^{1-}$ at 6500 cm^{-1} is quite small. The shift of g is highly dependent on metal spin−orbit coupling, with $g_z \sim 1.99$ for V,[42] and Mo, whereas $g_z = 1.9448$ for $[W(bdt)_3]^{1-}$. Alternatively, it could simply result from the inadequacy of a second-order perturbation treatment of coordination complexes with large metal spin−orbit couplings.

In the present case where the excitation energies are much greater than the ξ (even for tungsten) the A-values can be evaluated as described in eq 4, adapted from similar definitions by McGarvey[63] and Stiefel[18] assuming strict 3-fold symmetry generating an axial splitting. Here, P is the dipolar coupling parameter ($= g_e\mu_B g_n \mu_n \langle r^{-3}\rangle_{n,d}$) and κ represents the isotropic Fermi-contact component due to spin density at the nucleus. The second term echoes the dipole−dipole interaction from the electron residing in the $\psi_{z^2}^{a_1^*}$ ground state orbital, and the last term accounts from the small mixing of other d orbitals into the ground state (g-shifts).

$$A_{\parallel} = P[-\alpha^2\kappa + 4/7\beta^2 - 1/7\ (g_{\perp} - 2.0023)]$$

$$A_{\perp} = P[-\alpha^2\kappa - 2/7\beta^2 - 13/14\ (g_{\perp} - 2.0023)] \qquad (4)$$

Although there is a noticeable departure in the experimental data from axial symmetry, nonetheless this coarse approximation is sufficient to explore contributions to the magnetic hyperfine interaction; β is the covalency coefficient for the degenerate $\psi^{5e^*}{}_{x^2-y^2,xy}$ MOs that are considered M−S π^* bonds. For molybdenum, P is negative because the nuclear g_n is negative for the ^{95,97}Mo isotopes; the opposite sign occurs for ^{183}W.[64] With symmetry driven admixture of metal s character into the d_{z^2} ground state, the Fermi contact is the dominant contributor to the hyperfine expressions (eq 4). A similar conclusion resulted from the single-crystal EPR measurements of isoelectronic $[V^{IV}(mnt)_3]^{2-}$,[18] and is used to characterize the A-values for a host of $[V(dithiolene)_3]^{0/2-}$ complexes.[42] With vanadium being chemically related to molybdenum and tungsten by a diagonal relationship ("Schrägbeziehung") within the periodic system, isoelectronic tris(dithiolene)vanadium dianions serve as a useful counterpoint. The contribution of increased Mo/W−S covalency which instigates the positive shift of $g_{x,y}$ compared with the vanadium system also accounts for the stark differences in the anisotropy and magnitude of the hyperfine interaction. It can be noted in eq 4 that the anisotropy in $[V(dithiolene)_3]^{2-}$ stems from a dominant Fermi contact contribution that originates from direct s−d mixing (the $3a_1$ ground state is 86% $3d_{z^2}$ character with a 0.1% 4s contribution),[42] and polarization of the inner V 2s orbital concomitant with this large d character. These two contributions have opposing effects, with the dominant polarization of the 2s orbital effecting a large negative shift on the principal A-values and substantially overwhelming any positive contribution from 4s mixing. The dipolar contribution to the hyperfine, which stems from the π bonding mixing coefficient β, is large enough to counter both the isotropic and g-shift (negligible for V) contributions that render $A_{\parallel} \sim 0$.[18,42]

In contrast, Mo and W complexes exhibit larger s character in their $3a_1$ ground states due to an inherently smaller energy gap between nd and $(n + 1)$s levels for heavier transition metal ions because of relativistic effects.[51,65] However, the polarization of inner 3s and 4s orbitals by the Mo 4d and W 5d unpaired electron, respectively, is attenuated by both a decrease in the d character of the SOMO and more diffuse s orbitals as the principal quantum number is increased, therein diluting charge density at the nucleus. Therefore, the dominant contribution from polarized s orbitals is reduced with a concomitant increase in the s−d mixing that overall lowers the magnitude of the isotropic term in eq 4 since they oppose each other. The result is a substantial decrease in A-anisotropy with $A_{\parallel} \sim {}^1/_3 A_{\perp}$ in Mo and W complexes compared to the V species. Additionally, the magnitude of the dipolar term is reduced owing to the increased covalency, and increased g-anisotropy for these heavier metals leads to overall a smaller hyperfine interaction.

Type A Ligands. Monoanionic molybdenum tris(dithiolene) complexes where the dithiolene is olefinic exhibit near isotropic frozen solution spectra across all three frequencies (Figure 9b). Such a manifestation is a clear indication that the unpaired electron is no longer residing on the Mo ion, but rather delocalized across the ligand framework in line with a $[Mo^{IV}(^{A}L_3^{5-\bullet})]^{1-}$

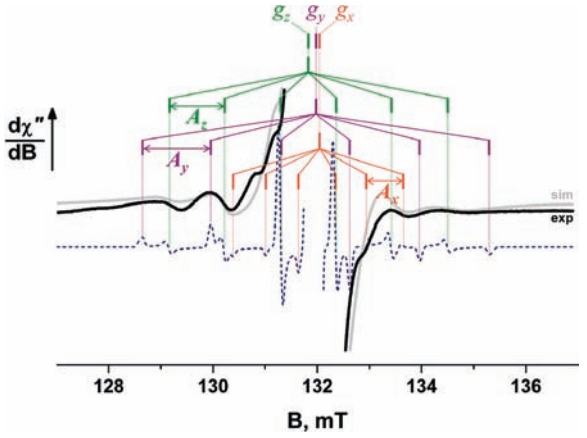

Figure 10. Magnification of the ^{95,97}Mo hyperfine features in the S-band spectrum of $[Mo(pdt)_3]^{1-}$ measured at 30 K. The experimental spectrum is shown in black with the simulation depicted by the light gray trace; the Mo $I = 0$ components are not shown for clarity. The simulation with sharp linewidths and no strain is shown beneath as the blue dashed line; the Mo $I = 0$ content has been removed. The principal components of the **g** and **A** are shown above the spectra with g_x/A_x in green, g_y/A_y in purple, and g_z/A_z in orange, revealing their individual contributions to the simulation.

formulation (Figure 7). The *g*-anisotropy is miniscule, an order of magnitude lower than their aryl-1,2-dithiolate counterparts, and all *g*-values are greater than g_e (Table 7). The axial symmetry is maintained in the **g** matrix, with the maximum value corresponding to $g_\parallel$ with only a very minor splitting of $g_\perp$, the opposite pattern to that seen with type B ligands (vide supra). For the asymmetrically substituted $(sdt)^{2-}$ ligand, different spin-Hamiltonian parameters will contribute to the overall spectral profile due to two isomers; however, these are not distinguishable even at S-band frequencies, and support the conclusion that the vast majority of the spin density is localized on the sulfur atoms of the ligand and not influenced by the ligand substituents. Contributions to the positive shift of the *g*-values stems from the reasonably large spin−orbit coupling constant for sulfur (ξ_S = 370 cm^{-1}),[60] witnessed previously with other S-based radicals.[66] We have refrained from conducting a similar analysis of the *g*-shifts using perturbation theory owing to the overwhelming complexity in the expressions due to the number of pertinent ligand p orbital permutations coming from the six sulfur and six carbon atoms of the tris(dithiolene) unit.

Molybdenum superhyperfine is present in the spectra of each complex, and clearly resolved at low frequency. Unlike **g**, the hyperfine interaction is weakly axial, and the approximate $A_x < A_y \sim A_z$ pattern (not found for $[Mo(sdt)_3]^{1-}$) suggests the **A** is rotated away from **g** such the larger *A*-values are aligned with the smaller *g*-values. This is emphasized in Figure 10, where we have delineated the three principal *g*- and *A*-values from the simulation of the S-band spectrum of $[Mo(pdt)_3]^{1-}$. By depicting the simulation of the ^{95,97}Mo $I = {}^5/_2$ spectral components with miniscule linewidths, it is clear that the unique *g*-value ($g_\parallel = g_z$) must be associated with one of the $A_\perp$-values; the smallest *g*-value (denoted g_x) is associated with the unique *A*-value, A_z. Although a pattern does emerge with the values in Table 7 that suggests a rotation of **A** ~90° about g_y (which maps A_x and A_z to the g_z and g_x matrix elements, respectively), there is a significant deviation from true axial splitting. In the absence of a single crystal EPR study we cannot make any assertions about the orientation of **g** and **A** with respect to the molecular frame. This misalignment is suggestive of orthorhombic symmetry and presumably a consequence of the SOMO consisting of six sulfur and six carbon atoms (Figure 8c) such that by virtue of its size, it is more prone to adopt different conformations in a frozen solution matrix that is responsible for the noted departures from true axial symmetry. At this stage, the experimental resolution is insufficient to classify this apparent noncoincidence as characteristic of a $2a_2'$ ground state.

Although the calculated ground state is devoid of metal character (Table 8, Figure 8c), polarization of M−S bonds deposits a small, yet significant, amount of spin density on the metal ion that generates the observed molybdenum superhyperfine (Figure 8d). A similar set of spin-Hamiltonian parameters was obtained from the very unique EPR spectrum of isoelectronic $[Re^V(dithiolene)_3]$, where an $(L_3)^{5-\bullet}$ encapsulates a low-spin Re(V) d^2 central ion.[19] The latter was characterized with a spectacularly large quadrupole interaction stemming from the large nuclear quadrupole moments for the ^{185,187}Re ($I = {}^5/_2$, 100% abundance) isotopes of 2.8 and 2.6 × 10^{-24} cm^2, respectively. Although the molybdenum ion in these complexes bears the same electron configuration, there is no apparent manifestation of quadrupole effects in the spectra due to a combination of low isotopic abundance of $I > 0$ isotopes (25.47%) and small nuclear quadrupole moments (−0.022 and 0.255 × 10^{-24} cm^2). Nevertheless, the near axial symmetry of **g** and **A** for both Mo and Re species suggests the trigonal prismatic geometry is maintained in solution. A substantial trigonal twist (D_3) or dithiolene fold (C_{3h}) ultimately leads to a metal-centered ground state that increases both the *g*-anisotropy and the hyperfine interaction.

This point is relevant to the experimental and theoretical observations for the analogous tungsten species. In contrast to the molybdenum complexes, the spectra for tris(dithiolene)-tungsten monoanions exhibit an obvious *g*-splitting at all three experimental frequencies such that the anisotropy is only a third of the value determined for $[W(bdt)_3]^{1-}$. This arises from a larger splitting of $g_\perp$ leaving $g_x < g_e$, and highlights an obvious ground state composition different to its group 6 congener. Interestingly, we consistently arrived at a C_{3h} symmetric structure with geometry optimization of $[W(mdt)_3]^{1-}$ starting from the crystal structure coordinates. As discussed above, this lowering of symmetry arises from folding of the dithiolene ligands along the S···S vector (Scheme 3) that destabilizes the ligand-centered $2a_2'$ MO with respect to the metal-centered $3a_1'$ MO but also facilitates mixing of these orbitals which transform as a' in C_{3h} point symmetry. Therefore, dithiolene folding installs W d_{z^2} character into the ground state, which DFT estimates to be 36% (Table 8). This would certainly account for the observed *g*-splitting, since these species would have a more oxidized central ion and therefore exhibit some of the spectral characteristics of $[W(bdt)_3]^{1-}$. It is difficult to attribute this anisotropy to the larger spin−orbit coupling constant for the heavier metal because we would expect a similar effect in the Re spectra whose own spin−orbit coupling constant is of equal magnitude.[19] Moreover, the tungsten hyperfine interaction is also much larger than for the analogous Mo or Re species, though it has the same axial symmetry and relative alignment. As a consequence, these spectra support the notion that the solution state structure for $[W^{IV}(^AL_3^{5-\bullet})]^{1-}$ is C_{3h} in stark contrast to the D_{3h} or D_3 symmetric geometries found by X-ray crystallography, and indicates a modest pliability of the structure to accommodate the demands of crystal packing. Certainly, more spectroscopic data are required

dx.doi.org/10.1021/ic2006265 |*Inorg. Chem.* 2011, 50, 7106–7122

before any firm conclusions can be drawn, though it appears tungsten's preference for higher oxidation states places the true electronic structure somewhere between the $[W^{IV}(^{A}L_3^{5-\bullet})]^{1-}$ and $[W^{V}(^{A}L_3^{6-})]^{1-}$ limiting forms.

A final consideration is for the complexes $[M(mnt)_3]^{1-}$ (M = Mo, W) bearing the cyano-substituted type A ligand. If redox potentials governed the allotment of complexes into different groups, then these two compounds would occupy a class of their own. One of the salient points documented by the computational analysis of Solomon and co-workers[20] was the energetic separation of the $3a_1''$ and $2a_2'$ MOs was substantially smaller for bdt_3 than mdt_3, which ultimately drove $[Mo(bdt)_3]^{1-}$ to a trigonally distorted structure. The decreased energy gap was attributed to the reduced π donation due to delocalization of charge density into the aromatic ring and away from the S-donor atoms. Although the $(mnt)^{2-}$ ligand appears as a type A ligand, the cyanide substituents are also conjugated into the C_2S_2 π system, which effects a large positive shift of the reduction potential[67] making highly reduced tris(dithiolene) complexes accessible.[48] The spin-Hamiltonian parameters for $[M(mnt)_3]^{1-}$ (M = Mo, W) are more axially symmetric than spectra with other type A ligands, indicating these ligands are more resistant to structural distortions due to the extensive π conjugation. Moreover, despite this, they have the same overall profile as the other complexes of this type, with miniscule *g*-anisotropy and equivalent metal superhyperfine coupling; therefore, a trigonal prismatic arrangement of the MS_6 polyhedron in solution is likely. The noticeably smaller anisotropy of $[W(mnt)_3]^{1-}$ compared with $[W(pdt)_3]^{1-}$ and $[W(mdt)_3]^{1-}$ may indicate a smaller distortion to C_{3h} symmetry, counterintuitively yielding an electronic structure closer to $[W^{IV}(^{A}L_3^{5-\bullet})]^{1-}$ with a more reduced tungsten ion.

CONCLUSIONS

A seminal sulfur K-edge XAS study by Solomon and co-workers disclosed a pronounced difference in the electronic structure of tris(dithiolene)molybdenum monoanions that depends on whether the ligand is of the olefinic type (type A, Scheme 1) or aromatic type (type B, Scheme 1).[20] In the present work, this difference has been confirmed by electronic absorption and EPR spectroscopy, which clearly reveal the existence of two classes of compounds. Type A systems bear a $[Mo(^{A}L_3^{5-\bullet})]^{1-}$ formulation with the unpaired spin delocalized over all three dithiolene ligands in the $2a_2'$ MO. This environment for the unpaired spin gives rise to almost isotropic EPR spectra that exhibit no noticeable anisotropy even at Q-band frequencies. Superhyperfine coupling to the molybdenum ion occurs via distribution of spin density through a modest polarization of Mo−S bonds, the same mechanism used by isoelectronic $[Re(L_3^{5-\bullet})]^{0}$.[19] The consequence of the oxidized ligand set is that the structures are (distorted) trigonal prismatic in the solid state. This coordination geometry is expected to persist in solution. For analogous tungsten monoanions, theoretical calculations predict a C_{3h} distorted trigonal structure that appears to be consistent with the trend of the spin-Hamiltonian parameters. The second-order Jahn−Teller distortion increases the tungsten contribution to the ground state and renders, if true, an electronic structure between the $[W^{IV}(^{A}L_3^{5-\bullet})]^{1-}$ and $[W^{V}(^{A}L_3^{6-})]^{1-}$ extremes. The type B complexes are consistently $[M^{V}(^{B}L_3^{6-})]^{1-}$ (M = Mo, W), with the central +V ion coordinated by three dianionic dithiolate(2-) ligands, and are completely analogous to isoelectronic $[V^{IV}(L_3^{6-})]^{2-}$. The different degree of *A*-anisotropy between the first-, second-, and third-row transition metal ions stems from a decreasing Fermi contact term, i.e., spin density at the nucleus, due to the increasing principal quantum number and relativistic effects. The metal−ligand bond covalency increases concomitantly, as it appears the Mo 4d and W 5d manifolds are more comparable energetically to the sulfur 3p orbitals of the tris(dithiolene) unit.

The electronic structure of the neutral species ($S = 0$) in these three-membered electron transfer series is still subject to differing descriptions. We have postulated $[M^{V}(^{B}L_3^{5-\bullet})]$ (M = Mo, W) for complexes possessing the $(tbbdt)^{2-}$ ligand,[13] the diamagnetic ground state being a result of strongly antiferromagnetically coupled metal and ligand unpaired electrons. This position was revised by Solomon and co-workers, who preferred a $[Mo^{IV}(^{A,B}L_3^{4-})]$ formulation in keeping with their S K-edge analysis and computational data.[20] The corresponding tungsten complexes were not examined.

It is important to recognize that all $[M(dithiolene)_3]^{0}$ crystal structures have C_{3h} symmetry brought about by large dithiolene folding (Scheme 3). In terms of distribution of valence electrons, the perfect trigonal prism has a $(4e')^4(3a_1')^2(2a_2')^0(5e')^0$ electron configuration with a d^2 central ion. A second-order Jahn−Teller distortion, whose magnitude is dependent on the $3a_1'-2a_2'$ energy separation,[20,45] will mix these MOs (the HOMO and LUMO), which transform as $3a'$ and $4a'$, respectively, in C_{3h} symmetry. Although the d_{z^2} orbital is stabilized, overall metal content is lost from the $3a'$ as was calculated for $[W(mdt)_3]^{1-}$, ensuring a more oxidized tungsten ion (vide supra). The folded conformation has a $(4e')^4(3a')^1(4a')^1(5e')^0$ electron configuration, as was observed for isoelectronic $[V^{IV}(^{A,B}L_3^{5-\bullet})]^{1-}$ ($S = 0$), where it appears strong antiferromagnetic coupling drives this distortion. Moreover, the lack of intensity in the first S K-pre-edge transition in neutral Mo (and W) complexes, compared to their Re analogues,[68] is accounted for by equal measures of metal and ligand content in the LUMO. Eventually, further folding will give an equal mix of metal and ligand character to the HOMO such that Pauli coupling (2e in one MO) will arise. In such a circumstance, an integer oxidation state cannot be applied.

Where precisely neutral tris(dithiolene) complexes of molybdenum and tungsten fit into the foregoing scheme is wholly dependent on the metal composition of the ground state (experiment or theoretical), which stems from the degree of ligand folding governed by the metal ion and ligand substituents. At this position of the periodic table, where covalency is dominant, it appears that the true electronic structure of the metal tris(dithiolene) complexes is best represented by the resonance structures $\{[M^{IV}(^{A,B}L_3^{4-})]^{0} \leftrightarrow [M^{V}(^{A,B}L_3^{5-\bullet})]^{0}\}$. As was observed with cobalt in its dithiolene complexes,[69] the molybdenum, and most probably tungsten, ions in neutral tris(dithiolene) species resist unambiguous physical oxidation state assignment and are to be regarded as finely nuanced cases that contrast with other systems in the larger body of metallodithiolene chemistry.

ASSOCIATED CONTENT

Supporting Information. X-ray crystallographic files in CIF format for **1**−**6** and $[NEt_4]_2[W(mdt)_3]$; cyclic voltammograms and electronic absorption spectra; fluid and frozen solution multifrequency EPR spectra for all monoanionic species, and their measuring conditions. Tables of geometric and electronic

dx.doi.org/10.1021/ic2006265 |*Inorg. Chem.* 2011, 50, 7106–7122

structures details (qualitative MO schemes and Mulliken spin density plots) of all calculated structures. This material is available free of charge via the Internet at http://pubs.acs.org.

AUTHOR INFORMATION

Corresponding Author

*E-mail: sproules@mpi-muelheim.mpg.de (S.S.).

Present Addresses

[§]Central Mechanical Engineering Research Institute, Mahatma Gandhi Avenue, Durgapur-713209, West Bengal, India.

ACKNOWLEDGMENT

This publication is dedicated to the memory of Prof. Edward I. Stiefel who pioneered the application of EPR spectroscopy to transition metal dithiolene chemistry. We are eternally grateful to Dr. Eckhard Bill for insightful discussions and repeatedly demonstrating a masterful command of the spin-Hamiltonian. This work is supported by NSF Grant CHE-0845289 (J.P.D.), IBM (fellowship support to Y.Y.), and the Fonds der Chemischen Industrie. S.S. and P.B. thank the Max-Planck-Society for postdoctoral fellowships. The Louisiana Board of Regents is thanked for enhancement grant LEQSF-(2002-03)-ENH-TR-67 with which Tulane's X-ray diffractometer was purchased, and Tulane University is acknowledged for its ongoing support with operational costs for the diffraction facility.

REFERENCES

(1) King, R. B. *Inorg. Chem.* **1963**, *2*, 641.

(2) Smith, A. E.; Schrauzer, G. N.; Mayweg, V. P.; Heinrich, W. *J. Am. Chem. Soc.* **1965**, *87*, 5798.

(3) Eisenberg, R.; Brennessel, W. W. *Acta Crystallogr.* **2006**, *C62*, m464.

(4) (a) Eisenberg, R.; Gray, H. B. *Inorg. Chem.* **1967**, *6*, 1844. (b) Eisenberg, R.; Ibers, J. A. *J. Am. Chem. Soc.* **1965**, *87*, 3776. (c) Eisenberg, R.; Ibers, J. A. *Inorg. Chem.* **1966**, *5*, 411.

(5) Boyde, S.; Garner, C. D.; Enemark, J. H.; Ortega, R. B. *J. Chem. Soc., Dalton Trans.* **1987**, 297.

(6) Boyde, S.; Garner, C. D.; Enemark, J. H.; Bruck, M. A.; Kristofzski, J. G. *J. Chem. Soc., Dalton Trans.* **1987**, 2267.

(7) Brown, G. F.; Stiefel, E. I. *J. Chem. Soc. D* **1970**, 728.

(8) Brown, G. F.; Stiefel, E. I. *Inorg. Chem.* **1973**, *12*, 2140.

(9) Cervilla, A.; Llopis, E.; Marco, D.; Pérez, F. *Inorg. Chem.* **2001**, *40*, 6525.

(10) (a) Draganjac, M.; Coucouvanis, D. *J. Am. Chem. Soc.* **1983**, *105*, 139. (b) Coucouvanis, D.; Hadjikyriacou, A.; Toupadakis, A.; Koo, S. M.; Ileperuma, O.; Draganjac, M.; Salifoglou, A. *Inorg. Chem.* **1991**, *30*, 754. (c) Heuer, W. B.; Mountford, P.; Green, M. L. H.; Bott, S. G.; O'Hare, D.; Miller, J. S. *Chem. Mater.* **1990**, *2*, 764. (d) Matsubayashi, G.; Douki, K.; Tamura, H. *Chem. Lett.* **1992**, *21*, 1251. (e) Matsubayashi, G.; Douki, K.; Tamura, H.; Nakano, M.; Mori, W. *Inorg. Chem.* **1993**, *32*, 5990. (f) Sugimoto, H.; Furukawa, Y.; Tarumizu, M.; Miyake, H.; Tanaka, K.; Tsukube, H. *Eur. J. Inorg. Chem.* **2005**, 3088. (g) Xu, H.-W.; Chen, Z.-N.; Wu, J. G. *Acta Crystallogr.* **2002**, *E58*, m631.

(11) (a) Cowie, M.; Bennett, M. J. *Inorg. Chem.* **1976**, *15*, 1584. (b) Friedle, S.; Partyka, D. V.; Bennett, M. V.; Holm, R. H. *Inorg. Chim. Acta* **2006**, *359*, 1427. (c) Harrison, D. J.; Lough, A. J.; Nguyen, N.; Fekl, U. *Angew. Chem.* **2007**, *119*, 7788. (d) Wang, K.; McConnachie, J. M.; Stiefel, E. I. *Inorg. Chem.* **1999**, *38*, 4334.

(12) Fomitchev, D.; Lim, B. S.; Holm, R. H. *Inorg. Chem.* **2001**, *40*, 645.

(13) Kapre, R. R.; Bothe, E.; Weyhermüller, T.; DeBeer George, S.; Wieghardt, K. *Inorg. Chem.* **2007**, *46*, 5642.

(14) Lim, B. S.; Donahue, J.; Holm, R. H. *Inorg. Chem.* **2000**, *39*, 263.

(15) Schulze Isfort, C.; Pape, T.; Hahn, F. E. *Eur. J. Inorg. Chem.* **2005**, 2607.

(16) McCleverty, J. A. *Prog. Inorg. Chem.* **1968**, *10*, 49.

(17) Davison, A.; Edelstein, N.; Holm, R. H.; Maki, A. H. *J. Am. Chem. Soc.* **1964**, *86*, 2799.

(18) Kwik, W.-L.; Stiefel, E. I. *Inorg. Chem.* **1973**, *12*, 2337.

(19) Sproules, S.; Benedito, F. L.; Bill, E.; Weyhermüller, T.; DeBeer George, S.; Wieghardt, K. *Inorg. Chem.* **2009**, *48*, 10926.

(20) Tenderholt, A. L.; Szilagyi, R. K.; Holm, R. H.; Hodgson, K. O.; Hedman, B.; Solomon, E. I. *Inorg. Chem.* **2008**, *47*, 6382.

(21) Makhaev, V. D.; Borisov, A. P.; Karpova, T. P.; Lobkovskii, E. B.; Tarasov, B. P.; Chekhlov, A. N. *Bull. Acad. Sci. USSR, Div. Chem. Sci.* **1989**, *38*, 377.

(22) Schrauzer, G. N.; Mayweg, V. P. *J. Am. Chem. Soc.* **1966**, *88*, 3235.

(23) Falaras, P.; Mitsopoulou, C.-A.; Argyropoulos, D.; Lyris, E.; Psaroudakis, N.; Vrachnou, E.; Katakis, D. *Inorg. Chem.* **1995**, *34*, 4536.

(24) McCleverty, J. A.; Locke, J.; Wharton, E. J.; Gerloch, M. *J. Chem. Soc. A* **1968**, 816.

(25) Stiefel, E. I.; Eisenberg, R.; Rosenberg, R. C.; Gray, H. B. *J. Am. Chem. Soc.* **1966**, *88*, 2956.

(26) Sellmann, D.; Kern, W.; Moll, M. *J. Chem. Soc., Dalton Trans.* **1991**, 1733.

(27) Goddard, C. A.; Holm, R. H. *Inorg. Chem.* **1999**, *38*, 5389.

(28) Sheldrick, G. M. *SADABS, Bruker-Siemens Area Detector Absorption and Other Corrections, Version 2006/1*; Universität Göttingen: Göttingen, Germany, 2006.

(29) *ShelXTL 6.14*; Bruker AXS Inc.: Madison, WI, 2003.

(30) Sheldrick, G. M. *ShelXL97*; Universität Göttingen: Göttingen, Germany, 1997.

(31) Hanson, G. R.; Gates, K. E.; Noble, C. J.; Griffin, M.; Mitchell, A.; Benson, S. *J. Inorg. Biochem.* **2004**, *98*, 903.

(32) Neese, F. *Orca, an Ab Initio, Density Functional and Semiempirical Electronic Structure Program Package, version 2.8*; Universität Bonn: Bonn, Germany, 2010.

(33) (a) Becke, A. D. *J. Chem. Phys.* **1993**, *98*, 5648. (b) Lee, C. T.; Yang, W. T.; Parr, R. G. *Phys. Rev. B* **1988**, *37*, 785.

(34) (a) van Lenthe, J. H.; Faas, S.; Snijders, J. G. *Chem. Phys. Lett.* **2000**, *328*, 107. (b) van Lenthe, E.; Snijders, J. G.; Baerends, E. J. *J. Chem. Phys.* **1996**, *105*, 6505. (c) van Lenthe, E.; van der Avoird, A.; Wormer, P. E. S. *J. Chem. Phys.* **1998**, *108*, 4783.

(35) Weigend, F.; Ahlrichs, R. *Phys. Chem. Chem. Phys.* **2005**, *7*, 3297.

(36) (a) Pulay, P. *Chem. Phys. Lett.* **1980**, *73*, 393. (b) Pulay, P. *J. Comput. Chem.* **1982**, *3*, 556.

(37) *Molekel, Advanced Interactive 3D-Graphics for Molecular Sciences, Swiss National Supercomputing Center*; http://www.cscs.ch/molkel.

(38) Schrauzer, G. N.; Finck, H. W.; Mayweg, V. P. *Angew. Chem.* **1964**, *76*, 715.

(39) Sproules, S.; Weyhermüller, T.; Wieghardt, K. Unpublished results.

(40) Bhattacharya, A. K.; Hortmann, A. G. *J. Org. Chem.* **1974**, *39*, 95.

(41) Banerjee, P.; Sproules, S.; Weyhermüller, T.; DeBeer George, S.; Wieghardt, K. *Inorg. Chem.* **2009**, *48*, 5829.

(42) Sproules, S.; Weyhermüller, T.; DeBeer, S.; Wieghardt, K. *Inorg. Chem.* **2010**, *49*, 5241.

(43) (a) Mahadevan, C.; Seshasayee, M.; Murthy, B. V. R.; Kuppusamy, P.; Manoharan, P. T. *Acta Crystallogr.* **1983**, *C39*, 1335. (b) Mahadevan, C.; Seshasayee, M.; Radha, A.; Manoharan, P. T. *Acta Crystallogr.* **1984**, *C40*, 2032.

(44) Sarangi, R.; DeBeer George, S.; Jackson Rudd, D.; Szilagyi, R. K.; Ribas, X.; Rovira, C.; Almeida, M.; Hodgson, K. O.; Hedman, B.; Solomon, E. I. *J. Am. Chem. Soc.* **2007**, *129*, 2316.

(45) Campbell, S.; Harris, S. *Inorg. Chem.* **1996**, *35*, 3285.

(46) Boyde, S.; Garner, C. D.; Joule, J. A.; Rowe, D. J. *Chem. Commun.* **1987**, 800.

(47) Wharton, E. J.; McCleverty, J. A. *J. Chem. Soc. A* **1969**, 2258.
(48) Best, S. P.; Ciniawsky, S. A.; Humphrey, D. G. *J. Chem. Soc., Dalton Trans.* **1996**, 2945.
(49) Best, S. P.; Clark, R. J. H.; McQueen, R. C. S.; Walton, J. R. *Inorg. Chem.* **1988**, *27*, 884.
(50) Stiefel, E. I.; Bennett, L. E.; Dori, Z.; Crawford, T. H.; Simo, C.; Gray, H. B. *Inorg. Chem.* **1970**, *9*, 281.
(51) Pyykkö, P. *Chem. Rev.* **1988**, *88*, 563.
(52) (a) Tucci, G. C.; Donahue, J. P.; Holm, R. H. *Inorg. Chem.* **1998**, *37*, 1602. (b) Holm, R. H.; Solomon, E. I.; Majumdar, A.; Tenderholt, A. L. *Coord. Chem. Rev.* **2011**, *255*, 993.
(53) Burrow, T. E.; Morris, R. H.; Hills, A.; Hughes, D. L.; Richards, R. L. *Acta Crystallogr.* **1993**, *C49*, 1591.
(54) (a) Kepert, D. L. *Inorg. Chem.* **1972**, *11*, 1561. (b) Stiefel, E. I.; Brown, G. F. *Inorg. Chem.* **1972**, *11*, 434.
(55) Beswick, C. L.; Schulman, J. M.; Stiefel, E. I. *Prog. Inorg. Chem.* **2004**, *52*, 55.
(56) The calculated total energy difference between optimized and crystallographic structures is a substantial 7 eV in favor of the former. However, this is quite unrealistic and indicates that the solvent and counterion effects not included in the calculation play a significant role in stabilizing the experimental minimum.
(57) Goodman, B. A.; Raynor, J. B. *Adv. Inorg. Chem. Radiochem.* **1970**, *13*, 135.
(58) Gardner, J. K.; Pariyadath, N.; Corbin, J. L.; Stiefel, E. I. *Inorg. Chem.* **1978**, *17*, 897.
(59) Sproules, S.; Wieghardt, K. Unpublished results.
(60) Mabbs, F. E.; Collison, D. *Electron Paramagnetic Resonance of d Transition Metal Compounds*; Elsevier: Amsterdam, 1992.
(61) Young, C. G.; Enemark, J. H.; Collison, D.; Mabbs, F. E. *Inorg. Chem.* **1987**, *26*, 2925.
(62) In true octahedral symmetry the metal d orbital coefficients (a for $d_{xz,yz}$; b for $d_{x^2-y^2,xy}$) are $a^2 = {}^2/_3$ and $b^2 = {}^1/_3$; in a perfect trigonal prism $a^2 = 1$ and $b^2 = 0$. For intermediate twist angles for D_3 symmetry species, a^2 lies somewhere between ${}^2/_3$ and 1. Although the complexes in question are not strictly octahedral, they are close enough to the octahedral limit to make this simplification valid.
(63) McGarvey, B. R. *Transition Met. Chem.* **1966**, *3*, 89.
(64) McGarvey, B. R. *Inorg. Chem.* **1966**, *5*, 476.
(65) Kuiper, D. S.; Douthwaite, R. E.; Mayol, A.-R.; Wolczanski, P. T.; Lobkovsky, E. B.; Cundari, T. R.; Lam, O. P.; Meyer, K. *Inorg. Chem.* **2008**, *47*, 7139.
(66) (a) Milsmann, C.; Bothe, E.; Bill, E.; Weyhermüller, T.; Wieghardt, K. *Inorg. Chem.* **2009**, *48*, 6211. (b) Lassmann, G.; Kolberg, M.; Bleifuss, G.; Gräslung, A.; Sjöberg, B.-M.; Lubitz, W. *Phys. Chem. Chem. Phys.* **2003**, *5*, 2442. (c) van Gastel, M.; Lubitz, W.; Lassmann, G.; Neese, F. *J. Am. Chem. Soc.* **2004**, *126*, 2237.
(67) Helton, M. E.; Gruhn, N. E.; McNaughton, R. L.; Kirk, M. L. *Inorg. Chem.* **2000**, *39*, 2273.
(68) Sproules, S.; Wieghardt, K. *Coord. Chem. Rev.* **2011**, *255*, 837.
(69) Ray, K.; Begum, A.; Weyhermüller, T.; Piligkos, S.; van Slageren, J.; Neese, F.; Wieghardt, K. *J. Am. Chem. Soc.* **2005**, *127*, 4403.